Paper status: Submitted

Why X-ray–Selected AGN Appear Optically Dull

J. R. Rigby[1], G. H. Rieke[1], J. L. Donley[1], A. Alonso-Herrero[1,2], P. G. Pérez-González[1], & S. P. Willner[3]

jrigby@as.arizona.edu

ABSTRACT

We investigate why half of X-ray–selected active galactic nuclei (AGN) in deep surveys lack signs of accretion in their optical spectra. The majority of these "optically–dull" AGN are no more than ~ 6 times fainter than their host galaxies in rest-frame R-band; as such, AGN lines are unlikely to be overwhelmed by stellar continuum in at least half the sample. We find that optically–dull AGN have the mid–infrared emission and L_x/L_{IR} ratios characteristic of local Seyferts, suggesting that the cause of optical dullness is not missing UV–optical continua. We compare the morphologies of 22 optically–dull and 9 optically–active AGN at $0.5 < z < 0.8$, and find that optically–dull AGN show a wide range of axis ratio, but optically–active AGN have only very round axis ratios. We conclude that hard X-rays select AGN in host galaxies with a wide range of inclination angle, but only those AGN in the most face-on or spheroidal host galaxies show optical emission lines. Thus, extranuclear dust in the host galaxy plays an important role in hiding the emission lines of optically–dull AGN.

Subject headings: galaxies: active—X-rays: galaxies—infrared: galaxies

1. Introduction

Deep X-ray surveys have found large numbers of active galactic nuclei (AGN) at $z \sim 1$, as predicted by models of the X-ray background. Most of these AGN have hard X-ray flux ratios that indicate obscured accretion, which is consistent with the hardness of

[1]Steward Observatory, University of Arizona, 933 N. Cherry Ave., Tucson, AZ 85721

[2]Instituto de Estructura de la Materia, Consejo Superior de Investigaciones Científicas, E-28006 Madrid, Spain

[3]Harvard–Smithsonian Center for Astrophysics, 60 Garden Street, Cambridge, MA, 02138

the X-ray background. In the local universe, AGN that are similarly X-ray obscured have optical high-excitation emission lines that classify them as Seyfert 2 galaxies. Surprisingly, in deep surveys, 40–60% of X-ray–selected AGN show **no evidence** of nuclear accretion in optical spectra (see discussion and references in Moran et al. 2002.) Such sources are variously termed "optically–dull", "optically–normal", or "X-ray–Bright Optically-Normal (XBONG)". By this, one means that these galaxies *lack evidence for accretion activity* in optical spectroscopy. They are therefore quite unlike a "normal" AGN, i.e. a QSO or Seyfert galaxy.[4]

Thus, what is so interesting about these AGN is precisely that they are "dull": How can nuclei produce high X-ray luminosities (most have $41 < \log L_x < 44$ erg s^{-1} in rest-frame 2–8 keV) that clearly require power from nuclear accretion, yet not show optical evidence of accretion? The puzzle deepens when we consider that optically-dull AGN are rare in the local universe. As we discuss in §5.1, at most 10–20% of local hard X-ray–selected AGN are optically dull. Has the AGN population evolved?

In this paper, we test three explanations for optical dullness: a) these AGN have weak ionizing continua, which do not excite the narrow line regions (e.g. Barger et al. 2001.) b) these are faint AGN in bright galaxies that overwhelm the AGN lines; c) the host galaxies of these AGN have obscured their AGN lines. Explanations b) and c) are effects seen in low–redshift samples, as we summarize in § 2. Explanation a) would require the AGN population to evolve strongly, from optical–dullness at $z \sim 1$ to optical activity at $z \sim 0$. Before appealing to AGN evolution, we should consider whether explanations b) and c), which are motivated by the behavior of local Seyferts, can fully explain optical dullness.

2. Insight from low–redshift Seyfert samples

Samples of nearby Seyferts suggest two likely causes for optical dullness in AGN. The first possible explanation is that optically–dull AGN have been observed in ways that dilute or hide their optical activity. This explanation was advanced by Moran et al. (2002), who observed 18 local Seyfert 2s with large apertures (to simulate observations at high redshift), and demonstrated that in 11 cases, the nuclear activity was drowned out by stellar light. (Nine of those sources showed early–type spectra, and two showed starburst spectra). This

[4]Terminology for deep X-ray sources can be confusing. "Optically dull" or "optically normal" AGN are X-ray–selected AGN that lack AGN emission lines, but otherwise have typical host galaxies. They are an entirely different population than the optically–bright X-ray–faint sources in deep surveys (in which the X-rays come from X-ray binaries, not AGN) which are sometimes called "normal galaxies."

"dilution" hypothesis predicts that optically–dull AGN should inhabit high–luminosity host galaxies, which generate enough continuum to drown out the AGN lines.

Another possible explanation is that the narrow–line regions of optically–dull AGN have been obscured by their host galaxies. This hypothesis is motivated by selection effects observed in local Seyfert samples. Keel (1980) first demonstrated a deficiency of nearby Seyfert 1s in edge-on host galaxies. McLeod & Rieke (1995) later showed that much larger samples of nearby optically–selected Seyfert 1 and 2 AGN are biased against having inclined spiral hosts. They found samples of soft X-ray–selected QSOs to be similarly biased. By contrast, they found that nearby samples of Seyferts selected by hard X-rays or 12 μm emission showed relatively flat distributions of axis ratio from 0.2 to 1, which is the expectation for randomly-oriented disk galaxies. Based on the known spatial scales of narrow-line regions, and on the differing biases of soft and hard–X-ray selected samples, they concluded that many Seyfert galaxies have several magnitudes of A_V at scale-heights of $\geq$ 100 pc—which puts the extinction outside the classical nuclear "torus". They proposed that molecular rings of star-forming disturbed gas could account for the obscuring column. (Alonso-Herrero et al. 2003 also invoked $A_V \lesssim 5$ of galactic extinction outside the torus, to explain the nuclear SEDs of optically–classified Seyfert 1.8 and 1.9 AGN.) Thus, the circumnuclear region is not the only absorbing column that matters to a nearby AGN; gas in the host galaxy matters too. This low redshift work suggests that at $z \sim 1$, where Chandra observes rest-frame hard X-rays, the deep surveys should select AGN independent of inclination. Inclined disk galaxies within these surveys should have preferentially weak broad- and narrow-lines. The relatively large fraction of optically–dull AGN at high redshift then arises from the comparatively low ratio of signal to noise in spectra of those faint objects, combined with the poor physical resolution to isolate their nuclei. Are these trends observed?

3. Sample selection and data

To investigate optically–dull behavior, we need a uniform sample of such AGN at $z \sim 1$. We start with the Szokoly et al. (2004) catalog of X-ray–selected AGN with spectroscopic redshifts, all in the Chandra Deep Field South (CDFS). These AGN were originally selected from the Chandra 1 Ms observations (Giacconi et al. 2002; Alexander et al. 2003), and were followed up with optical spectroscopy (Szokoly et al. 2004) obtained with the FORS1/FORS2 at the VLT ($R = 5.5$ Å pix^{-1}). In this paper we use both the Szokoly et al. (2004) catalog and electronic versions of their published spectra, available online[5].

[5]http://www.mpe.mpg.de/CDFS/data/

From the spectroscopic catalog, we select AGN with X-ray luminosities that indicate AGN activity (which corresponds to Szokoly X-ray classifications of AGN-1, AGN-2, QSO-1, or QSO-2). We then select the subset of those sources that have non–active optical spectral classifications: either "LEX" (sources with low–excitation narrow emission lines, as expected from star formation) or "ABS" (sources with stellar absorption–line spectra). These criteria select 45 sources, all of which have a spectroscopic redshift; 34 of these redshifts are listed as "reliable" (flag Q= 3). Nine of the 45 sources have "ABS" spectra, and the rest have "LEX" spectra. Table 1 lists source positions, redshifts, optical spectral classifications, and X-ray classifications, all from Szokoly et al. (2004). We use source identification numbers from Alexander et al. (2003), abbreviated "AID".

We also list, in table 1, several derived quantities for each source: 1) rest–frame 2–8 keV luminosity (using the photon index inferred from the observed 0.5–2 keV / 2–8 keV flux ratio, and normalizing by the observed 2–8 keV flux); 2) the absorption-corrected rest-frame 2–8 keV X-ray luminosity, which we find by extrapolating the observed 2–8 keV flux assuming an intrinsic photon index $\Gamma = 2$, where $f_\nu \propto \nu^{1-\Gamma}$; and 3) the estimated column density N_H, which would make an intrinsic $\Gamma = 2$ power-law spectrum at the given redshift show the observed 0.5–2 keV / 2–8 keV flux ratio. When the source was not detected in the hard (2–8 keV) band, we quote upper limits on N_H, L_x, and absorption–corrected L_x. When the source was not detected in the soft (0.5–2 keV) band, we quote an upper limit on N_H. The median N_H errorbar, from the uncertainty in the X-ray flux ratio, is 35%.

From the same catalog, we also create a comparison sample of "optically–active AGN": X-ray–selected AGN that have either broad emission lines ("BLAGN") or high-excitation narrow emission lines ("HEX") according to Szokoly et al. (2004). Observed and derived quantities are listed in table 2.

Having selected a sample, we assembled a multiwavelength photometric database. Using *Spitzer* (Werner et al. 2004), we obtained IRAC (Fazio et al. 2004) images of the CDFS with 500 s of integration. The images were reduced by the *Spitzer* Science Center using the standard pipeline. We also obtained MIPS (Rieke et al. 2004) 24 μm scan map images with a total integration time of $\sim$ 1400 s per position, nominally composed of 120 individual sightings per source. These data were reduced using the instrument team data analysis tool (Gordon et al. 2005), creating the image presented by Rigby et al. (2004).

We add the following optical and near–infrared imagery: ACS/HST *bviz* images from GOODS (Giavalisco et al. 2004); *RIz* frames from the Las Campanas Infrared Survey (Marzke et al. 1999); *BVRI* images released by the ESO Imaging Survey (Arnouts et al. 2002); *JK* images from GOODS (Giavalisco et al. 2004); and *JK* images from the EIS Deep

Infrared Survey[6].

Unlike optically–faint AGN (Rigby et al. 2005), optically–dull AGN have relatively bright, unambiguous optical and near–infrared counterparts. Therefore, creating SEDs is straightforward. The result is closely–sampled, deep photometry from 0.4 to 8 μm, with additional coverage at 24 μm. We classify the 0.4–8 μm SEDs into 5 categories, based on the Devriendt et al. (1999) templates: old stellar population; young stellar population; intermediate-age stellar population; flat in νf_ν; or rising in νf_ν with increasing wavelength. We deliberately ignore 24 μm flux density when classifying, as it can be elevated by star formation or accretion. Table 1 lists the SED classifications.

Using these data, we now examine the three most likely explanations for optical dullness: a) weak ionizing continua; b) dilution by the host galaxy continuum; and c) obscuration.

We adopt an $\Omega_m = 0.26$, $\Omega_\Lambda = 0.74$, $h_o = 0.72$ cosmology throughout. When we take luminosities and absolute magnitudes from the literature, we convert them to this cosmology.

4. Do optically–dull AGN have weak ionizing continua?

One of the proposed causes for optical dullness is intrinsically weak ionizing continua, such that the narrow line regions are not excited. We perform two tests of this hypothesis.

4.1. Do the low-obscuration AGN have big blue bumps?

First, do low–X-ray obscuration AGN show the "big blue bumps" (Filippenko 1988) attributed to normal, UV–bright accretion disks? Such low–X-ray obscuration AGN are likely to have low–extinction lines of sight to the nucleus, and thus are likely to show bright blue continua if they have accretion disks. However, differential extinction along the different lines of sight to the optical and X-ray components could result in a lack of big blue bumps. How many of the X-ray–soft (and therefore presumably low obscuration) AGN in the sample have indications of "big blue bumps"? Of the 10 AGN with lowest estimated column densities ($N_H < 3 \times 10^{22}$ cm^{-2}), only 2 have flat νf_ν SEDs; the rest have stellar SEDs that fall quickly in the blue.[7] So among these presumably low-obscuration AGN, big blue bumps appear to be rare. This is consistent with dust extincting the blue continuum, or with an intrinsically

[6]http://www.eso.org/science/eis/surveys/strategy_EIS-deep_infrared_deep.html

[7]Nine of the ten sources have reliable redshifts according to Szokoly et al. (2004).

weak blue continuum, although it is more difficult to explain under the dilution hypothesis.

There are indeed 14 sources with flat or probably flat SEDs—if these are not the lowest–column sources, what are they? Of the 14, 7 have low–reliability spectral quality flags (Szokoly et al. 2004); emission lines may well show up in better–quality spectra, and thus these sources may not be true "optically–dull AGN".

Thus, blue non–stellar SEDs are not common in the optically–dull sample, consistent with their having weak UV continua but also with their having UV of normal strength but obscured along our sightline. We need another test to distinguish these possibilities.

4.2. Do the SEDs of optically–dull AGN show normal mid-IR emission?

If the UV continua of the optically–dull objects really are weak, then the mid–IR emission should be abnormally weak for AGN. Local Seyferts characteristically have bright mid-IR emission (c.f. Spinoglio & Malkan 1989, Rush et al. 1993, Spinoglio et al. 1995, Maiolino et al. 1995) that is attributed to heating of dust by UV energy from the central engine. Assuming similarity in other regards, AGN with weak UV should also have weak IR. However, since dust heated by star formation also emits in the mid–infrared, we must choose our tests and samples carefully.

To first order, most of the rest–frame optical/near–IR SEDs in the sample are stellar. We select two subsamples that are unlikely to be dominated in the mid–infrared by emission from star-formation. As subsample A, we select the 9 optically–dull AGN whose optical spectra are dominated by absorption lines. Of these, seven have old stellar SEDs.[8] This subsample should be the least contaminated by star formation. We create subsample B by selecting optically–dull AGN whose SEDs (in observed $0.4 < \lambda < 8$ μm) are dominated by old stars, but whose spectra show low–excitation emission lines that indicate some HII regions are present. Eight optically–dull sources match these criteria.

In figures 1, 2, and 3 we plot the SEDs of the optically–dull AGN. Compared to an Sa galaxy template (Devriendt et al. 1999), 5 of 7 subsample A (ABS) sources show elevated 24 μm emission, as do 6 of 8 subsample B sources. Thus, this test supports the presence of significant UV luminosity. However, this simple test is not definitive because the templates do not reflect the observed range of SEDs observed with *Spitzer*. Additionally, the SED test

[8]The other two, AID 126 and 247, have power-law SEDs, but both have low–quality spectra (Szokoly et al. (2004) flags of 1.0 and 0.5, respectively), and thus may not have been classified as ABS given better spectra.

is not clear-cut for the subsample B sources, which by definition contain some low–level star formation that could elevate the 24 μm flux density.

4.3. Do optically–dull AGN have stellar or AGN-like Hβ/24 μm ratios?

Since Balmer emission and mid–infrared flux density are both strongly influenced by the star formation rate, we can use the observed Hβ emission–line flux to predict the observed 24 μm flux density predicted by star formation, and test whether the optically–dull AGN violate this expectation (by having 24 μm excess.)

We obtain optical emission line fluxes using the VLT spectra of Szokoly et al. (2004) discussed in § 3. For the two subsamples, the VLT spectra cover [O II λ3727], and generally cover all of the Balmer series except Hα. In subsample A, no source shows Balmer emission; 4/7 show Balmer absorption, and 3/7 show non-existent or very weak Balmer lines. Only 1 of 8 subsample B sources show Hβ emission; the rest have non–detected Balmer lines.

We fit continua at the Balmer lines and sum line fluxes. When Balmer lines are not detected or appear in absorption, we take a conservative upper limit on emission flux as f(Hβ)=3 $\times$ 10^{-16}erg s^{-1}(which is the fiveσ limiting Hβ emission flux of the spectrum with lowest signal-to-noise ratio). We deredden the Balmer fluxes by a standard extinction value[9] of E(B-V)= 0.435.

In figure 4 we plot the observed $f_\nu(24\ \mu\mathrm{m})/f(H\beta)$ ratios for subsamples A and B (lower panel), as well as for several comparison samples (upper panel). The first comparison sample is a sample of star-forming galaxies at $z \sim 0.7$, generated by cross-correlating the Hβ catalog of Lilly et al. (2003) with a 24 μm catalog obtained from our GTO *Spitzer* images of the Extended Groth Strip. The second is a sample of low-redshift PG quasars, with 24μm flux densities taken from the MIPS GTO AGN survey (D. Hines, private communication) and Hβ fluxes from Marziani et al. (2003); these quasars are unlike our sample in that they are generally unobscured AGN. The third sample consists of radio galaxies and quasars from Shi et al. (2005); the radio galaxies are more like our optically–dull sample in that their nuclei are obscured.

We also plot the Chary & Elbaz (2001) star-forming galaxy models with bolometric luminosities from 10^9 L$_\odot$ to 10^{12} L$_\odot$ (see appendix for details on the K-correction), along with the K-correction paths of two median PG quasar SEDs, the Elvis, Risaliti, & Zamorani

[9]This corresponds to $A_{H\alpha}$ = 1.1 and $A_{H\beta}$ = 1.57. It is the extinction value applied by Roussel et al. (2001), and is the average extinction observed by Kennicutt (1998).

(2002) template and the normalized (at $\lambda_{rest} = 25$ μm), de-redshifted median photometry of the Haas et al. (2003) sample.

There are several points to take from figure 4.

First, the galaxies from Lilly et al. (2003) are in the general range of the predictions of the Chary & Elbaz (2001) models. This suggests that the empirical relation between Hβ and mid–infrared flux density in star-forming galaxies at $z \sim 0$ (Roussel et al. 2001) holds reasonably well out to $z \sim 1$.

Second, at least two optically–dull AGN have $f_\nu(24\ \mu\mathrm{m})/f(H\beta)$ ratios that are too high to be consistent with star formation. These are the highest of the upward–pointing arrows, i.e., those with $\log f_\nu(24\ \mu\mathrm{m})/f(H\beta) > 15.4$ mJy/(erg s^{-1} cm^{-2}). *Thus, we see strong mid–infrared evidence of accretion in a few optically–dull AGN* from the 24 μm/Hβ test.

Third, the $f_\nu(24\ \mu\mathrm{m})/f(H\beta)$ ratio *is not* a useful diagnostic of AGN versus star formation activity for most of these sources. The problem is, the range of ratios seen for $0.5 < z < 1$ star-forming galaxies overlaps with the range seen in PG quasars and radio galaxies. Therefore, the ratio for the optically–dull galaxies are consistent with AGN–powered IR excesses, but the majority of sources have ratios that could also arise from star formation.

4.4. Do optically–dull AGN have AGN-like Mid-IR to X-ray luminosities?

The previous two subsections have shown that some optically–dull AGN appear to have AGN–powered excess 24 μm emission. The rest are consistent with this possibility, but differential extinction and inadequate comparison templates make arguments based on optical SEDs or Hβ line strength inconclusive for many of these galaxies. Therefore, we now compare the mid–infrared and X-ray luminosities of the optically–dull AGN, since both should be robust to large amounts of obscuration.

In figure 5 we plot the ratio of the absorption–corrected rest–frame 2–10 keV luminosity to the rest-frame 6 μm luminosity, as a function of estimated column density. We calculate rest-frame $\nu L_\nu(6\ \mu\mathrm{m})$ by extrapolating from the observed 24 μm flux density, assuming $\mathrm{f}_\nu \propto \nu^{-1}$)[10]. Figure 5 should be compared with figure 7 of Lutz et al. (2004), which is the corresponding plot for ~ 40 nearby active galaxies with *ISO* spectra.

[10]Very similar luminosities are obtained if we instead calculate 6 μm luminosity by interpolating between the observed 24 μm and 8 μm flux densities.

The first insight to gain from figure 5 is that the $z \sim 0.7$ AGN behave much like the low–redshift AGN of Lutz et al. (2004). The range of L_x/L_{IR} is similar (apart from a few outliers at low L_x/L_{IR}). Lutz et al. (2004) showed that the luminosity ratio does not depend on column density for local AGN; this finding constrains unification geometry, since many unification models predict a dependence on N_H. The CDFS sample shows that L_x/L_{IR} of AGN does not depend on column density at $z \sim 0.7$, either, a result first indicated by Rigby et al. 2004 from flux ratios, and also demonstrated by figure 9 of Alonso-Herrero et al. (2005).)

The second insight is that the optically–dull and optically–active AGN in the CDFS do not have significantly different L_x/L_{IR} ratios. Specifically, figure 5 does *not* show that optically–dull AGN have abnormally low mid–infrared luminosities given their X-ray luminosities. This result, along with those of the previous two section, argues strongly that *optically–dull AGN have Seyfert–like mid–infrared emission.*

The third insight is that the sources with young and old stellar SEDs do not have significantly different L_x/L_{IR}. This tentatively suggests that the scatter in L_x/L_{IR} for AGN is not primarily caused by emission from star formation. It is unknown what causes the considerable scatter in L_x/L_{IR}; both quantities should be reasonably robust to extinction and other line-of-sight effects.

Last, we note that the CDFS AGN include a handful with lower L_x/L_{IR} than seen by Lutz et al. (2004).

Thus, we conclude that the optically–dull AGN have X-ray and mid-IR luminosities within the normal ranges seen for local Seyferts. The SED and 24 μm/Hβ tests are consistent with the behavior seen in the L_x/L_{IR} test, and in some cases independently corroborate it. We conclude that *optically–dull AGN have the normal mid–IR emission expected for Seyfert galaxies.* This argues that optically–dull AGN have normal AGN blue and UV continua, to produce a normal AGN mid-IR luminosity. Thus, the lack of big blue bumps in the X-ray–soft AGN is probably not caused by intrinsically weak optical and UV continua.

5. How important is dilution to optical dullness?

We now estimate quantitatively the importance of "dilution" (bright galaxy continua overwhelming lines from faint AGN) in causing optical dullness. Dilution has been argued to be important in local samples of weak–line AGN, and so we first examine how similar these local AGN are to the $z \sim 1$ optically–dull AGN. Next, we examine the optical-to-X-ray flux and luminosity ratios, to estimate the importance of dilution in our $z \sim 1$ sample.

5.1. Are optically–dull AGN at $z \sim 1$ like weak-line AGN at $z \sim 0$?

Several studies have searched for local examples of optically–dull AGN, since such sources are amenable to detailed follow-up. These searches generally obtain optical spectroscopy for sources in wide-area hard-band X-ray surveys, and identify the handful that lack optical emission lines. Several examples:

1. The 2–10 keV–selected HEAO-1 sample (Piccinotti et al. 1982) contains 39 sources that are not galaxy clusters; 30 of these have emission–line signatures of AGN, 7 were not identified with known sources, and only 1 corresponds to a non-active (i.e., an optically–dull) galaxy.

2. Follow-up spectroscopy of 5–10 keV Hellas Beppo-SAX sources found optical counterparts for 61/74 sources; 6 are apparently AGN without optical AGN signatures (La Franca et al. 2002) and have emission-line EW(Hβ)$\sim$ 1–5 Å.

3. The ASCA 2–10 keV Medium Sensitivity Survey identified 28 sources at $z < 0.2$ (Akiyama et al. 2003). All are broad-line, narrow-line, or BL Lac AGN, but five have weak emission lines (Hβ and [O III] equivalent widths below 10Å), and consequently might look optically-dull at higher redshift.

4. Watanabe et al. (2002) followed up the hardest 2% of the ASCA detections, and found three ($z \sim 0.05$) sources with $N_H \sim 10^{23}$ cm^{-2} and abnormally low–luminosity Seyfert/LINER emission lines. At redshifts typical of the deep surveys, these 3 sources should look like optically–dull AGN.

5. Using a different search method, Hornschemeier et al. (2005) correlated Chandra images with spectroscopy from the Sloan Digital Sky Survey. They found no X-ray sources that lacked optical signs of nuclear accretion. However, 4 of their 19 AGN would not be identified as AGN through optical spectroscopy if their redshifts exceeded ~ 0.5.

Although it is not always clear for these studies whether additional members of the sample would appear optically–dull at high redshift, they agree that locally, optically–dull AGN are not common in samples selected on the basis of X-ray emission.

In figure 6 we plot the column densities and redshifts of these local AGN[11]. For comparison, we also plot inferred column densities for the CDFS optically–dull AGN (see §3).

[11]Hornschemeier et al. (2005) and Piccinotti et al. (1982) do not list flux ratios, so we cannot infer a column density.

Figure 6 clearly demonstrates that many low–redshift AGN with weak emission lines have very low ($< 10^{22}$ cm^{-2}) column densities, much lower than the CDFS AGN. Since they are so much less obscured, they are not true analogues to the sources in the deep fields, and so the importance of dilution to local weak–line AGN should not argue for the importance of the effect in very different AGN at $z \sim 1$.

Thus, dilution may be important for the low–column, local AGN with weak lines; but the much higher column densities of the CDFS AGN argue, at the very least, that these populations are not similar. This opens the possibility that extinction or other effects may be more important for the distant AGN than for local weak–line AGN.

5.2. X-ray to optical flux and luminosity ratios

To further understand the importance of dilution to distant optically–dull AGN, in figure 7 we plot the observed R-band and 2–8 keV fluxes of the CDFS sample. This figure should be compared to figure 3 of Comastri et al. (2002). Comastri et al. (2002) looked at ten $z \sim 0.2$ optically–dull AGN from HELLAS2XMM and Chandra (Barger et al. 2001), and found that most have high f_r/f_x ratios—which suggests that they have very luminous host galaxies (which makes spectral dilution likely.) In contrast, our figure 7 demonstrates that this effect is *not* common for the 45 CDFS optically–dull AGN: all but a handful have optical/X-ray flux ratios that are typical of AGN. Thus, this plot does not support the dilution hypothesis for optically–dull AGN in the CDFS.

However, figure 7 is not an ideal diagnostic tool, since it uses observed fluxes and thus does not K–correct. Accordingly, in figure 8 we plot the rest–frame absolute R magnitudes and rest-frame absorption–corrected 2–8 keV luminosities of the optically–dull sample. (We also plot the local–universe weak-line AGN from figure 6, and the optically–active AGN in the CDFS.) In each panel of figure 8, the thick diagonal line shows the M_R/L_x ratio of the composite radio-quiet QSO SED from Elvis, Risaliti, & Zamorani (2002). The thin diagonal lines mark flux ratios 10 and 100 times brighter in the optical than the QSO M_R/L_x ratio. Panel b of figure 8 shows the M_R/L_x ratios of the optically–active AGN; 96% of those sources lie above the 10× Elvis line; as such, their AGN should contribute at least 10% of their optical luminosities, and in many cases should dominate. Comparison with panel c then shows that 67% of the optically–dull sources have M_R/L_x ratios above the 10× Elvis line. A more restrictive cut would be the 6.3× Elvis line: 94% of the optically–active sources fall above it; and 56% optically–dull sources do.

Thus, we conclude, based on figures 7 and 8, that the R-band to X-ray luminosity ratios

suggest that less than half of the optically–dull AGN are dull because a bright galaxy drowns out the AGN optical flux. However such dilution is likely at work in the optically–dull AGN whose total (AGN+host) optical luminosities are $\gtrsim 6$ times brighter than the X-rays the AGN should be; this effect may be important for local weak–line AGN. Thus, we conclude that dilution is only a plausible explanation for half or less of the CDFS optically–dull AGN. We need a cause for optical–dullness in the remaining half.

6. Can Host Galaxy Obscuration Cause Optical–Dullness in AGN?

Having shown that spectral dilution cannot account for the optical dullness of half the sample, and that the ionizing continua are unlikely to be missing given the normal mid-IR luminosities, we now examine the role that host galaxy obscuration may play in causing optical dullness. To do this, we examine the axis ratios of the optically–dull and optically–active AGN in the CDFS. Most (80%) of the optically–dull AGN lie within the ACS GOODS survey described by Giavalisco et al. (2004). These deep, high–resolution images provide morphology information even on distant sources. In the following analysis, we use the i-band images from the v1.0 public release of the GOODS ACS images. Measured axis ratios of most sources vary by only a few percent among the v, i, and z-band catalogs; therefore, we are free to choose the i-band, to optimize depth and spatial resolution (sampling rest-frame optical light at $z \sim 0.7$).

6.1. Measuring Axis Ratios

For each AGN, we measure the axis ratio, b/a, using two methods.

First, we simply take the b/a values from the GOODS v1.0 public release i-band Source Extractor catalogs. While Source Extractor (Bertin & Arnouts 1996) is not optimized for morphological parameter fitting, it is a widely-available tool that can quickly estimate axis ratios for thousands of galaxies, and thus is of potential interest for large surveys.

Second, we iteratively fit multi-component Galfit models (Peng et al. 2002, Galfit v2.0.3b) to each source. This method is more time-consuming, but potentially more robust in its measurement of b/a than Source Extractor. We fit the following four Galfit models to each source:

- a point source, i.e. the HST PSF (which we created from stars in the GOODS i-band images).

- a single Sersic component.
- a point source plus a Sersic component.
- a deVaucouleurs component plus an exponential disk component.

We adopted the b/a ratio of the best-fitting model, as follows:

- If the PSF provided the best fit, we considered the source to be unresolved, and so we have no knowledge of the true b/a ratio.
- If the Sersic or PSF+Sersic models fit best, we adopted the Sersic component's b/a.
- If the bulge+disk model fit best, and both components had effective radii greater than the PSF FWHM, then we adopted as b/a the weighted mean of the two component b/a values, weighted by the fluxes of the model components. If only one component had $R_e >$ FWHM, then we used the b/a value of that component. (Since any $R_e <$ FWHM component is essentially unresolved, the b/a value galfit assigns it is not meaningful.) (This weighting may over-estimate b/a in very inclined galaxies, since the bulge will generally be rounder than the disk.)

When sources were fit well by more than one Galfit model, the axis ratios of the models agreed well. Also, the b/a values measured by Source Extractor and Galfit are quite similar for each source, though Galfit tends toward smaller b/a ratios since it can fit multiple components. We quote axis ratios from Galfit unless otherwise indicated.

6.2. Axis Ratios of the $0.5 < z < 0.8$ Subsample

We can now compare the axis ratios of the optically–dull and optically–active AGN. We must take care because the luminosity and redshift distributions of the two samples differ. Specifically, the optically–active AGN tend to be more luminous and lie at higher redshift, and therefore are more likely to be unresolved or have limited morphology information. To minimize this selection bias, we consider the subsample of optically–dull and optically–active AGN with GOODS coverage that have redshifts between 0.5 and 0.8[12]. Because this includes the "redshift spike" in the CDFS, the subsample contains more sources than one

[12]All of the optically–active sources in this redshift range have reliable redshifts, and all but 3/22 of the optically–dull sources do.

would expect in an average field: there are 22 optically–dull AGN, and 9 optically–active AGN[13]. The absorption–corrected X-ray luminosity distributions of these two samples are comparable.

Tables 3 and 4 list the measured axis ratios for the optically-dull and active samples. Figure 9 shows cutouts of the GOODS i-band images for the $0.5 < z < 0.8$ AGN. Figure 10 plots the axis ratio distributions. Clearly, the b/a distributions of the two samples are very different: the optically–active galaxies are round, and the optically-dull galaxies have a range of b/a.

Let us explore the differences between these distributions in more detail. *All the* $0.5 < z < 0.8$ *optically–active sources are less concentrated than the PSF* (using concentration parameter $C = 5 \log r_{80}/r_{20}$ from Kent 1985), and half are much less concentrated. Of the optically–active AGN, all but one have b/a$>$ 0.79 [14]. Only two sources, AID 88 and 94, show complicated (and perhaps disturbed) morphologies. Only one source (AID 103) shows any evidence for a possible inclined disk.

The optically–dull AGN are also all resolved. By contrast with the optically–active AGN, the optically–dull AGN show a range of axis ratio: $0.26 < b/a < 0.89$.One source is possibly interacting (AID 196), and there are two irregulars (48 and 60). Of the spirals, 3 are highly inclined (AID 44, 134, 146); 2 are close to face-on (AID 139, 176) and 2 have intermediate inclinations (AID 91, 157, 269). The two–sided Kolmogorov-Smirnov test disproves, at 99.7% confidence, the null hypothesis that the optically-dull and optically–active $0.5 < z < 0.8$ AGN are drawn from the same parent distribution.

Is the optically–active sample biased by nuclear point sources toward high axis ratios? This question arises since 6/9 have broad emission lines, and four of these galaxies are centrally concentrated, though not as much as a PSF. Therefore, for each optically–active AGN in our $0.5 < z < 0.8$ sample, we measure the *maximum* flux that could come from a central point source, assuming no galaxy emission. The maximal PSF flux is, in the median, 25% of the total source flux, and corresponds to $i_{AB} = 22.36$. We then add a PSF of this median brightness, with Poisson noise, to the centroid of each optically–dull source, and repeat the galfit axis ratio measurements. Figure 10 shows the result: adding artificial point sources to the optically–dull AGN means that some sources are no longer fit well by any model; but most sources are still fit acceptably, and the resulting b/a distribution does *not* resemble the optically–active distribution. Galfit is able to fit the artificial point source and

[13]Three are narrow-line AGN (88, 179, and 241), and the rest are broad-line AGN.

[14]The one exception is AID 88, whose complicated morphology may indicate an interaction.

still correctly measure the axis ratio of the galaxy.

Thus, we conclude that the host galaxies of optically–dull AGN more fully sample the expected range of random inclination angles than do optically–active AGN.

6.3. Additional Axis Ratios from $z < 0.5$ and $z > 0.8$ AGN

Though the $0.5 < z < 0.8$ redshift sample should be the most robust against luminosity–related morphological bias, we do have morphological information on the rest of the sample, and we now briefly examine it. Since this sample may be biased, it should not be used to argue that the optically–dull AGN have a more diverse distribution of axis ratio than the optically–active AGN. But if the trends from the previous section are not present in the full redshift range, that would weaken the evidence that the trends are real.

Twenty-five optically–active AGN in the CDFS have GOODS ACS imaging and $z < 0.5$ or $z > 0.8$. Most (17) of these are well-fit by a point source (of which 8 show some faint extended emission after PSF subtraction.) Thus, only eight sources have morphology information: one PSF + ring galaxy (with b/a= 0.6); two compact but resolved galaxies; two sources that appear to be undergoing interactions (AID 193 and 214); and three irregular galaxies. Their b/a ratios are listed in table 4.

There are 15 optically-dull AGN with GOODS imaging and $z < 0.5$ or $z > 0.8$. Of these, only 3 are point sources, 4 are irregular or interacting galaxies, and the remaining 8 sources have b/a ratios from 0.2 to 0.9. The K-S test finds that the any–redshift optically–dull and any–redshift optically–active samples are drawn from different populations, at 99.5% significance. Thus, the higher and lower redshift sources do not contradict the results of the $0.5 < z < 0.8$ sample.

6.4. Column density evidence for extra obscuration

If host galaxy obscuration is a cause of optical dullness, then we might expect higher X-ray column densities for the optically–dull AGN than the optically–active. In figure 11 we plot the column density distributions for the optically–dull and optically active sources with absorption–corrected L_x below 10^{44} erg s^{-1}. The optically–dull sources appear to have higher column densities, as expected if the host galaxy contributes extra extinction. This result is marginally significant: the two–sided Kolmogorov-Smirnov test estimates a 95% probability that the two distributions are drawn from different parents. Adding back in the high–luminosity sources would increase the significance. Host galaxies are not expected to

create a large amount of extra X-ray column, given the ROSAT extinction relation $A_V = N_H/(1.8 \times 10^{21})$ mag cm^{-2} (Cox 2000).

7. Discussion

We showed in §4 that optically–dull AGN do not have unusually weak ionizing continua; we instead found that optically–dull AGN have normal Seyfert (UV–powered) mid–infrared emission (and thus the optical may be the only wavelength range where these AGN appear odd). Further, in §5 we demonstrated (by comparing the rest–frame hard X-ray and optical luminosities) that dilution by stellar continuum is unlikely to explain the optical dullness of at least half our sample. We thus needed a primary cause for optical dullness in the majority of the sample.

In §6 we show that obscuration by host galaxies is a likely cause of optical dullness for these AGN, which can explain the missing emission lines and big blue bumps, and the normal Seyfert–like X-ray and mid-IR emission. We did this by showing that the host galaxies of X-ray–selected AGN have a range of axis ratio consistent with a wide range of inclination angle, but that the subset with optical emission lines have a much narrower range of b/a, which is consistent with occuring either in nearly face-on galaxies, or in spheroid–dominated galaxies. Since at $z = 1$, the observed 2–8 keV band samples rest–frame 4–16 keV energies, the Chandra–selected AGN in the deep fields really are selected by hard X-rays, and thus it is not surprising that they, like local hard X-ray–selected samples, show a large range of axis ratio. Redshift will also act to increase the net obscuration in the observed optical wavelengths of these sources, which should increase the disparity between optically–selected and hard X-ray–selected samples. In addition, bright diagnostic lines like $H\alpha$ are redshifted out of the optical bands, further increasing the disparity. Therefore, we propose that the selection effects demonstrated in McLeod & Rieke (1995) for local AGN explain many of the "optically–dull" AGN: they are missing narrow emission lines due to absorption by extranuclear dust in their host galaxies.

This behavior has been modeled by Maiolino & Rieke (1995) (see their figure 3). They show that the expected distribution for an unbiased sample of b/a ratios for randomly oriented disk galaxies is very similar to the distribution of b/a ratios we measure in figure 10 using Galfit. They also demonstrate that, when observations are deep enough to provide a virtually complete sample independent of orientation, then the distribution of b/a for local Seyfert galaxies follows this distribution. The local Type 1 galaxies all have b/a near 1, while the galaxies with significantly smaller b/a are observed to be preferentially types 1.8, 1.9, and 2, thus directly demonstrating the influence of obscuration in the galaxy disk.

To be precise, the obscuration hypothesis predicts that b/a should be biased against face-on galaxies. Such a bias is not seen in figure 10, although the sample size is too small to test the detailed shape of the distribution. The handfull of high b/a sources in the $0.5 < z < 0.8$ optically–dull sample are consistent with having spectral dilution explain their optical dullness; they are centrally concentrated, and have higher–than–average M_R/L_x (at low significance given the small sample size).

Maiolino & Rieke (1995) also demonstrated that the proportion of missing AGN—or optically dull X-ray sources—depends critically on the quality of the spectra used for classification. For the nearby Seyferts in the Revised Shapley Ames catalog, the bias is almost absent, while there is a strong bias in the more distant CfA sample. The small proportion of optically dull X-ray galaxies in recent studies, as described in §5.1, is probably a result of the high quality spectra that can be obtained on relatively nearby galaxies.

For standard dust-to-gas ratios, this picture suggests that a considerable fraction of the column that obscures the soft X-rays may come from outside the obscuring torus. This complicates attempts to interpret X-ray column as a proxy for accretion disk inclination, as well as attempts to use obscured-to-unobscured AGN ratios to estimate torus geometries. In this picture, X-ray column is not solely a description of the nuclear obscuration, but of the galactic obscuration as well. This complex extinction geometry should be included in studies relating high–redshift AGN to the X-ray background, for example.

Also, this picture may partially explain the lack of dependence of the hard X-ray to 24 μm flux ratio on the X-ray hardness ratio (a proxy for column density). If many X-ray sources are partially obscured by gas and dust far away from the AGN, then the dust will not be heated sufficiently to emit in the mid–infrared. Thus, having the obscuration take place in the host galaxy as well as the torus will dilute the signatures of torus obscuration that were searched for, but not seen, in Rigby et al. (2004) and Lutz et al. (2004).

8. Conclusions

We have investigated the column densities, X-ray and IR luminosities, and morphologies of 45 X-ray–selected AGN in the CDFS that lack optical AGN emission lines (and are thus termed "optically–dull AGN".)

We test whether these sources are low–luminosity AGN in very luminous galaxies; this would support the hypothesis that the AGN emission lines are drowned out by bright galactic continua ("dilution"). Fifty-six percent of our sample have rest frame R-band luminosities no more than ~ 6 times larger than that expected for the AGN (scaling from the X-ray

luminosity), and thus *we conclude that dilution is not the primary cause of optical dullness* for at least half the sample. This should be contrasted with the bright $z \sim 0.2$ optically–dull AGN of Comastri et al. (2002), which have high optical–to–X-ray flux ratios that make dilution likely.

About half of the local weak–line AGN have column densities much lower than those of the CDFS sample ($\log N_H < 22$ cm^{-2}). In addition, it has been shown that dilution can account for the optical dullness of many of these low-redshift galaxies. Thus, they are not true analogues to the $z \sim 1$ population.

Optically–dull AGN have the normal mid–infrared emission we expect from Seyfert galaxies; in short, they look like AGN at 24 μm. Since AGN IR emission is powered by UV continua, it is likely that they have normal amounts of UV emission.

We test whether the morphologies of optically–dull AGN are atypical. The optically–dull AGN have host galaxies with a large range of inclination angle, whereas the optically–active AGN hosts are nearly–face-on spirals or spheroids (and thus should have less dust extinction). From this, we conclude that X-ray–selected AGN in deep fields are selected fairly independently of their inclination angle, but that only the most face-on or spherical show optical emission lines. In the rest, extranuclear dust in the host galaxy may obscure the narrow-line regions. This scenario is consistent with samples of Seyferts in the local universe, where hard X-ray and mid-IR–selected samples have unbiased b/a distributions, but optically–selected samples of Seyfert 1 and 2 AGN are systematically biased against inclined disk galaxies.

Thus, part of the column density that obscures the soft X-rays may come from the host galaxy, outside the obscuring torus. This complicates using the X-ray column to infer torus properties. It may also partially explain why the mid–infrared to X-ray luminosity ratio does not depend on column density in AGN.

Thus, we conclude that host galaxy obscuration is the primary cause of optical dullness, with spectral dilution a likely contributor for sources with high optical to absorption–corrected X-ray luminosity ratios.

A. Appendix: K-correcting model 24 μm/Hβ ratios

We predict how K-corrections should affect the observed $f_\nu(24\ \mu\mathrm{m})/f(H\beta)$ ratio, as follows. We redshift each Chary & Elbaz (2001) model to find the observed 24 μm flux density normalized to the rest–frame 15 μm flux density; this is a K-correction and thus

depends on redshift and SED shape. We normalize to 15 μm in order to take advantage of the empirical relation between 15 μm and Balmer emission measured by Roussel et al. (2001), which, combining equations from Roussel et al. (2001) and Kennicutt (1998), we can write as follows:

$$\Big(\frac{f_\nu(15\ \mu\mathrm{m})^{rest}}{f(H\beta)^{rest}}\Big) = \Big(\frac{14\times10^{26}}{\Delta\nu_{ISO}}\Big)\frac{mJy}{erg\ s^{-1}\ cm^{-2}} \tag{A1}$$

where $\Delta\nu_{ISO} = 6.75\times10^{12}$ Hz.

We can now combine this 15 μm–Balmer relation with the K-correction to calculate how the observed $f_\nu(24\ \mu\mathrm{m})/f(H\beta)$ ratio changes as the source is moved to higher redshift.

$$\Big(\frac{f_\nu(24\ \mu\mathrm{m})^{obs}}{f(H\beta)^{obs}}\Big) = \Big(\frac{f_\nu(15\ \mu\mathrm{m})^{rest}}{f(H\beta)^{rest}}\Big)\Big(\frac{f_\nu(24\ \mu\mathrm{m})^{obs}}{f_\nu(15\ \mu\mathrm{m})^{rest}}\Big) \tag{A2}$$

In figure 4 we plot this result, the expected $f_\nu(24\ \mu\mathrm{m})/f(H\beta)$ ratios for Chary & Elbaz (2001) models.

We thank G. Szokoly for kindly providing electronic versions of the VLT spectra in advance of online publication. This work is based in part on observations made with *Spitzer*, which is operated by the Jet Propulsion Laboratory, California Institute of Technology under NASA contract 1407. Support for this work was provided by NASA through Contract Numbers 960785 and 1256790 issued by JPL/Caltech.

REFERENCES

Akiyama, M., Ueda, Y., Ohta, K., Takahashi, T., & Yamada, T. 2003, ApJS, 148, 275

Alexander, D. M., et al. 2003, AJ, 126, 539

Cox, A. N. 2000, Allen's astrophysical quantities, 4th ed. Publisher: New York: AIP Press; Springer, 2000

Alonso-Herrero, A., et al. 2005, ApJ, submitted

Alonso-Herrero, A., Quillen, A. C., Rieke, G. H., Ivanov, V. D., & Efstathiou, A. 2003, AJ, 126, 81

Arnouts, S., Vandame, B., Benoist, C., Groenewegen, M. A., da Costa, L., Schirmer, M., Mignani, R. P., & Slijkhuis, R. 2002, VizieR Online Data Catalog, 337, 90740

Barger, A. J., Cowie, L. L., Mushotzky, R. R., & Richards, E. A. 2001, AJ, 121, 662

Bertin, E. & Arnouts, S. 1996, A&AS, 117, 393

Chary, R. & Elbaz, D. 2001, ApJ, 556, 562

Comastri, A. et al.2002, astro-ph/0203019

Devriendt, J., Guiderdoni B. & Sadat, R. 1999, A&A, 350, 381

Donley, J. L. et al., submitted

Elbaz, D., Cesarsky, C. J., Chanial, P., Aussel, H., Franceschini, A., Fadda, D., & Chary, R. R. 2002, A&A, 384, 848

Elvis, M., Risaliti, G., & Zamorani, G. 2002, ApJ, 565, L75

Fadda, D., Flores, H., Hasinger, G., Franceschini, A., Altieri, B., Cesarsky, C. J., Elbaz, D., & Ferrando, P. 2002, A&A, 383, 838

Fazio, G. G., et al. 2004, ApJS, 154, 10

Filippenko, A. V. 1988, Advances in Space Research, 8, 5

Fiore, F., et al. 2001, MNRAS, 327, 771

Giacconi, R., et al. 2002, ApJS, 139, 369

Giavalisco, M., et al. 2004, ApJ, 600, L93

Gordon, K., et al.2005 PASP, 117, 503

Hammer, F., et al. 1997, ApJ, 481, 49

Haas, M. et al. 2003, A&A, 402, 87

Hornschemeier, A. E., Heckman, T. M., Ptak, A. F., Tremonti, C. A., & Colbert, E. J. M. 2005, AJ, 129, 86

Keel, W. C. 1980, AJ, 85, 198

Kennicutt, R. C. 1998, ARA&A, 36, 189

Kent, S. M. 1985, ApJS, 59, 115

Kuraszkiewicz, J. K. et al. 2003, ApJ, 590, 128

La Franca, F. et al. 2002, ApJ, 570, 100

Lilly, S. J., Carollo, C. M., & Stockton, A. N. 2003, ApJ, 597, 730

Lutz, D., Maiolino, R., Spoon, H. W., & Moorwood, A. F. 2003, A&A, 418, 465

Maiolino, R., Ruiz, M., Rieke, G. H., & Keller, L. D. 1995, ApJ, 446, 561

Maiolino, R. & Rieke, G. 1995, ApJ, 454, 95

Marziani, P., Sulentic, J. W., Zamanov, R., Calvani, M., Dultzin-Hacyan, D., Bachev, R., & Zwitter, T. 2003, ApJS, 145, 199

Marzke et al. 1999, in PASP Conf. Ser. 191: Photometric Redshifts and Detection of High Redshift Galaxies, 148

McLeod, K. K. & Rieke, G. H. 1995, ApJ, 441, 96

Moran, E. C., Filippenko, A. V., & Chornock, R. 2002, ApJ, 579, 71

Peng, C. Y., Ho, L. C., Impey, C. D., & Rix, H.-W. 2002, AJ, 124, 266

Piccinotti, G., Mushotzky, R. F., Boldt, E. A., Holt, S. S., Marshall, F. E., Serlemitsos, P. J., & Shafer, R. A. 1982, ApJ, 253, 485

Rieke, G. H., et al. 2004, ApJ, 154, 25

Rigby, J. R., et al. 2004, ApJS, 154, 160

Rigby, J. R., Rieke, G. H., Pérez-González, P. G., Donley, J. L., Alonso-Herrero, A., Huang, J.-S., Barmby, P., & Fazio, G. G. 2005, ApJ, 627, 134

Rousell, H., Sauvage, M., Vigroux, L., & Bosma, A. 2001, A&A, 372, 427

Rush, B., Malkan, M. A., & Spinoglio, L. 1993, ApJS, 89, 1

Severgnini, P. et al.2003, A&A, 406, 483

Shi, Y. et al.2005, ApJ, in press

Silva, L., Maiolino, R., Granato, G. L. 2004, MNRAS, 255, 973

Spinoglio, L., & Malkan, M. A. 1989, ApJ, 342, 83

Spinoglio, L., Malkan, M. A., Rush, B., Carrasco, L., & Recillas–Crus, E. 1995, ApJ, 453, 616

Szokoly, G. P., et al. 2004, ApJS, 155, 271; catalog at http://www.mpe.mpg.de/CDFS

Watanabe, S., Akiyama, M., Ueda, Y., Ohta, K., Mushotzky, R., Takahashi, T., & Yamada, T. 2002, PASJ, 54, 683

Werner, M. W., et al. 2004, ApJS, 154, 1

Zezas, A., Alonso-Herrero, A., & Ward, M. J. 2001, Ap&SS, 276, 601

Table 1. Optically–Dull AGN

AID	SID	A-RA	A-DEC	S-RA	S-DEC	off	2-8 keV flux	log f(H)/f(S)	f_ν 24 μm	L_x	corr L_x	est N(H)	X class	Opt	Q	z	SED
12	121	52.96316	−27.84766	52.96316	−27.84766	0.0	1.4(±0.4) E-15	$0.47^{+0.13}_{-0.19}$	< 96	1.8E42	2.6E42	1.9E22	AGN-2	LEX	3	0.674	O
16	76	52.96875	−27.83819	52.96870	−27.83822	0.2	8.6(±0.7) E-15	$0.73^{+0.05}_{-0.05}$	87 ± 30	9.3E43	3.9E44	3.2E23	QSO-2	LEX	1	2.394	F
28	73	52.99208	−27.80944	52.99175	−27.80963	1.3	4.8(±0.5) E-15	$0.43^{+0.05}_{-0.05}$	82 ± 9	7.9E42	1.1E43	2.0E22	AGN-1	LEX	3	0.734	O
44	66	53.01520	−27.76769	53.01529	−27.76772	0.3	1.7(±0.1) E-14	$1.44^{+0.06}_{-0.07}$	126 ± 30	7.5E42	2.2E43	1.1E23	AGN-2	LEX	3	0.574	O
48	267	53.02037	−27.69100	53.02029	−27.69100	0.3	5.7(±1) E-15	> 1.38	91 ± 10	3.8E42	1.3E43	> 1.4E23	AGN-2	LEX	1	0.720	F
60	155	53.03295	−27.71091	53.03325	−27.71094	0.9	1.2(±0.4) E-15	$0.71^{+0.15}_{-0.22}$	520 ± 20	8.3E41	1.4E42	3.3E22	AGN-2	LEX	3	0.545	R
65	538	53.03541	−27.78016	53.03562	−27.78011	0.7	1.1(±0.3) E-15	> 1.10	990 ± 80	2.1E41	3.4E41	> 4.6E22	AGN-2	LEX	3	0.310	O
80	535	53.04758	−27.78050	53.04758	−27.78055	0.2	1.3(±0.3) E-15	$0.76^{+0.12}_{-0.16}$	< 80	9.8E41	1.7E42	3.7E22	AGN-2	LEX	3	0.575	O
83	534	53.05062	−27.75825	53.05087	−27.75838	0.9	< 4.8 E-16	< 0.87	< 80	< 6.9E41	< 9.3E41	< 6.2E22	AGN-2	LEX	3	0.676	O
84	149	53.05104	−27.77247	53.05125	−27.77272	1.1	1.3(±0.3) E-15	$0.94^{+0.14}_{-0.20}$	239 ± 40	2.5E42	7.3E42	1.2E23	AGN-2	LEX	1	1.033	Y
87	156	53.05504	−27.92469	53.05512	−27.92463	0.3	7.0(±0.9) E-15	> 1.77	116 ± 10	5.6E42	5.5E43	> 4.2E23	AGN-2	ABS	3	1.185	I
90	600	53.05762	−27.75711	53.05783	−27.75736	1.1	8.1(±3) E-16	> 1.21	< 80	1.6E42	8.4E42	> 2.7E23	AGN-2	LEX	3	1.327	I
91	266	53.05779	−27.71338	53.05775	−27.71361	0.8	1.2(±0.4) E-15	> 1.22	289 ± 40	9.9E41	3.0E42	> 1.2E23	AGN-2	LEX	3	0.735	Y
126	50	53.07912	−27.79872	53.07916	−27.79872	0.1	2.3(±0.4) E-15	$0.86^{+0.09}_{-0.11}$	< 80	2.2E42	4.4E42	5.4E22	AGN-2	ABS	1	0.670	F
129	525	53.08254	−27.68975	53.08250	−27.68966	0.3	< 9.4 E-16	< 0.62	3018 ± 90	< 1.1E41	< 1.4E41	< 1.6E22	AGN-2	LEX	3	0.229	O
131	253	53.08362	−27.74638	53.08366	−27.74644	0.2	4.2(±0.5) E-15	$1.55^{+0.12}_{-0.16}$	333 ± 30	1.3E42	3.6E42	1.2E23	AGN-2	LEX	1	0.481	F?
134	151	53.08529	−27.79233	53.08533	−27.79230	0.2	7.6(±0.7) E-15	$2.06^{+0.15}_{-0.22}$	65 ± 20	2.2E42	1.1E43	2.2E23	AGN-2	LEX	3	0.604	O
139	602	53.09141	−27.78219	53.09158	−27.78216	0.5	3.3(±1) E-16	> 0.82	222 ± 70	4.7E41	6.3E41	> 5.0E22	AGN-2	ABS	3	0.668	O
146	188	53.09400	−27.83050	53.09400	−27.83050	0.0	6.3(±2) E-16	$0.86^{+0.16}_{-0.25}$	69 ± 10	7.0E41	1.5E42	6.4E22	AGN-2	LEX	3	0.734	F
155	49	53.10095	−27.69066	53.10104	−27.69069	0.3	3.1(±0.4) E-15	$0.23^{+0.06}_{-0.07}$	68 ± 9	2.9E42	3.4E42	5.8E21	AGN-1	LEX	3	0.534	O
157	598	53.10283	−27.90325	53.10283	−27.90322	0.1	< 5.5 E-16	···	< 80	< 6.4E41	< 8.5E41	···	AGN-2	ABS	3	0.617	I
161	47	53.10416	−27.68383	53.10404	−27.68377	0.5	5.5(±0.8) E-15	$1.25^{+0.11}_{-0.15}$	155 ± 10	4.2E42	1.3E43	1.3E23	AGN-2	LEX	3	0.733	Y
162	260	53.10466	−27.84538	53.10462	−27.84536	0.2	1.3(±0.3) E-15	$1.24^{+0.16}_{-0.24}$	30 ± 10	1.8E42	7.7E42	1.9E23	AGN-2	LEX	3	1.043	F
164	150	53.10487	−27.91377	53.10483	−27.91391	0.5	3.9(±0.6) E-15	> 1.67	108 ± 30	3.3E42	2.5E43	> 3.4E23	AGN-2	ABS	3	1.090	O
166	45	53.10700	−27.71827	53.10700	−27.71825	0.1	4.9(±0.5) E-15	$0.66^{+0.05}_{-0.06}$	480 ± 50	5.7E43	2.0E44	2.4E23	QSO-2	LEX	1	2.291	R
171	519	53.10770	−27.91875	53.10779	−27.91844	1.1	< 7.8 E-16	< 0.64	63 ± 10	< 2.1E42	< 4.3E42	< 5.8E22	AGN-2	LEX	3	1.034	F
176	43	53.11150	−27.69600	53.11150	−27.69600	0.0	3.7(±0.5) E-15	$0.78^{+0.07}_{-0.08}$	385 ± 40	4.4E42	8.7E42	5.4E22	AGN-2	LEX	3	0.734	I
196	516	53.13058	−27.79027	53.13083	−27.79019	0.9	< 3.7 E-16	< 0.71	116 ± 8	< 5.1E41	< 6.8E41	< 3.9E22	AGN-1	LEX	3	0.665	F
212	512	53.14329	−27.73061	53.14312	−27.73063	0.5	6.8(±2) E-16	$0.59^{+0.15}_{-0.23}$	< 80	7.9E41	1.3E42	2.8E22	AGN-2	LEX	3	0.668	O
216	171	53.14629	−27.73627	53.14662	−27.73655	1.5	< 4.3 E-16	< 0.54	202 ± 40	< 1.0E42	< 1.4E42	< 3.3E22	AGN-2	LEX	1	0.839	F
220	190	53.14933	−27.68333	53.14941	−27.68322	0.5	5.4(±0.8) E-15	> 1.62	< 80	3.0E42	1.3E43	> 1.9E23	AGN-2	LEX	3	0.735	O
221	100	53.14991	−27.81397	53.14991	−27.81400	0.1	3.1(±1.3) E-16	$0.17^{+0.16}_{-0.27}$	43 ± 9	2.6E42	3.1E42	9.9E21	AGN-1	LEX	1	1.309	F
227	33	53.15295	−27.73508	53.15329	−27.73533	1.4	8.6(±0.6) E-15	$0.33^{+0.03}_{-0.03}$	94 ± 20	1.2E43	1.6E43	1.1E22	AGN-1	LEX	3	0.665	I
247	25	53.17016	−27.92961	53.17020	−27.92972	0.4	9.3(±0.8) E-15	$1.24^{+0.06}_{-0.07}$	661 ± 50	5.6E42	1.5E43	9.5E22	AGN-2	ABS	0.5	0.625	R
259	132	53.18358	−27.91502	53.18337	−27.91502	0.7	8.4(±3) E-16	$0.55^{+0.15}_{-0.24}$	< 80	1.9E42	3.4E42	3.5E22	AGN-2	LEX	1	0.908	F?
264	85	53.18587	−27.80991	53.18583	−27.80997	0.2	1.3(±0.3) E-15	$0.45^{+0.09}_{-0.11}$	< 80	2.9E43	7.1E43	1.5E23	QSO-1	LEX	1	2.593	F
269	170	53.19329	−27.90383	53.19337	−27.90388	0.3	1.4(±0.4) E-15	$0.79^{+0.13}_{-0.18}$	218 ± 30	1.3E42	2.6E42	4.7E22	AGN-2	ABS	3	0.664	O
271	252	53.19575	−27.72950	53.19595	−27.72966	0.9	2.9(±0.5) E-15	$1.39^{+0.15}_{-0.22}$	< 80	3.8E42	2.2E43	2.9E23	AGN-2	LEX	3	1.178	Y
274	18	53.19941	−27.70911	53.19958	−27.70911	0.5	3.0(±0.1) E-14	$0.57^{+0.02}_{-0.02}$	1114 ± 10	7.7E43	1.4E44	4.5E22	QSO-1	LEX	3	0.979	F?
276	184	53.20075	−27.88236	53.20075	−27.88244	0.3	2.0(±0.4) E-15	$1.11^{+0.14}_{-0.21}$	156 ± 30	1.5E42	3.7E42	8.6E22	AGN-2	ABS	3	0.667	O
285	242	53.21595	−27.70802	53.21600	−27.70822	0.7	< 1.5 E-15	< 0.62	437 ± 30	< 5.3E42	< 8.1E42	< 5.5E22	AGN-1	LEX	3	1.027	Y
298	110	53.24429	−27.77569	53.24420	−27.77555	0.6	< 8.3 E-16	< 0.43	< 80	< 9.4E41	< 1.3E42	< 1.5E22	AGN-1	LEX	3	0.622	F
303	12	53.24858	−27.84172	53.24870	−27.84177	0.5	4.3(±0.5) E-15	$0.21^{+0.05}_{-0.05}$	< 80	7.4E41	7.9E41	3.0E21	AGN-1	ABS	3	0.251	O
304	10	53.24904	−27.77394	53.24904	−27.77400	0.2	9.2(±0.7) E-15	$0.97^{+0.05}_{-0.06}$	108 ± 30	3.3E42	5.8E42	4.4E22	AGN-2	LEX	3	0.424	O
324	176	53.28829	−27.74688	53.28854	−27.74722	1.4	2.7(±0.8) E-15	$0.44^{+0.12}_{-0.17}$	125 ± 30	5.2E42	7.7E42	2.1E22	AGN-1	LEX	3	0.786	Y

Columns: (1) X-ray source identification from Alexander et al. (2003). (2) Source ID from Szokoly et al. (2004), which is identical to the Giacconi et al. (2002) XID. (3)–(4) RA and DEC (J2000) of the X-ray source, from Alexander et al. (2003) (5)–(6) RA and DEC (J2000) of the optical counterpart, from Szokoly et al. (2004). (7) Offset between X-ray and optical coordinates, in arcseconds. (8)–2-8 keV X-ray flux in erg s^{-1} cm^{-2}, from Alexander et al. (2003). (9) log of the 2–8kev / 0.5–2 keV flux ratio. (10) observed MIPS f_ν (24 μm) in μJy. (11) rest-frame 2–8 keV X-ray luminosity, using the photon index inferred from the 2–8kev / 0.5–2 keV flux ratio, and the 2–8 keV flux for normalization. (12) absorption-corrected rest-frame 2–8 keV X-ray luminosity, extrapolated from the observed 2–8 keV flux, assuming an intrisic photon index $\Gamma = 2$ and concordence cosmology ($\Omega_m = 0.27$, $\Omega_\Lambda = 0.73$, $h = 0.72$). (13) Estimated column density: the column density which would produce the observed 2–8kev / 0.5–2 keV flux ratio, given an intrinsic $\Gamma = 2$ power-law spectrum. (14)–(17) X-ray source classification, optical source classification, redshift quality flag, and redshift, all from Szokoly et al. (2004). (18) SED classification, this paper: O=old stellar population; Y=young stellar

Table 2. Optically–Active AGN

AID	SID	A-RA	A-DEC	S-RA	S-DEC	off	2-8 keV flux	log f(H)/f(S)	f_ν 24 μm	L_x	corr L_x	est N(H)	X class	Opt	Q	z
5	238	52.94991	−27.84597	52.94987	−27.84597	0.1	3.4(±0.5)E-15	$0.14^{-0.07}_{+0.08}$	< 80	1.8E43	2.1E43	6.5E21	AGN-1	BLAGN	3	1.065
14	112*a*	52.96658	−27.89075	52.96641	−27.89094	0.9	<1.3E-15	< 0.67	340 ± 10	< 2.3E43	< 9.9E43	< 3.8E23	QSO-2	HEX	3	2.940
18	230	52.97312	−27.81197	52.97312	−27.81197	0.0	<8.0E-16	< 0.33	< 80	< 1.6E43	< 2.9E43	< 6.4E22	AGN-1	BLAGN	3	2.185
22	75	52.98079	−27.91325	52.98075	−27.91344	0.7	1.7(±0.2)E-14	$1.13^{-0.08}_{+0.10}$	73 ± 13	1.5E43	4.2E43	1.1E23	AGN-2	HEX	3	0.737
34	71	53.00158	−27.72211	53.00145	−27.72211	0.4	7.0(±0.6)E-15	$0.29^{-0.04}_{+0.05}$	100 ± 10	2.9E43	3.9E43	1.6E22	AGN-1	BLAGN	3	1.037
39	68	53.00662	−27.72419	53.00658	−27.72416	0.2	5.6(±0.5)E-15	$0.31^{-0.04}_{+0.05}$	< 80	1.9E44	3.4E44	8.8E22	QSO-1	BLAGN	3	2.726
41	67	53.01025	−27.76675	53.01029	−27.76677	0.2	8.6(±0.6)E-15	$0.30^{-0.04}_{+0.04}$	200 ± 50	9.5E43	1.4E44	3.0E22	QSO-1	BLAGN	3	1.616
43	117	53.01262	−27.74738	53.01270	−27.74727	0.5	9.0(±3)E-16	$0.12^{-0.12}_{+0.16}$	< 80	3.9E43	4.9E43	2.1E22	QSO-1	HEX	3	2.573
63	89	53.03433	−27.69822	53.03450	−27.69822	0.5	<8.1E-16	< 0.23	< 80	< 2.6E43	< 4.0E43	< 4.5E22	AGN-1	BLAGN	3	2.47
66	63	53.03608	−27.79288	53.03616	−27.79288	0.3	6.8(±0.1)E-14	$0.18^{-0.01}_{+0.01}$	3300 ± 100	6.8E43	7.6E43	4.3E21	QSO-1	BLAGN	3	0.543
68	62	53.03937	−27.80188	53.03941	−27.80188	0.1	6.0(±0.5)E-15	$0.73^{-0.05}_{+0.05}$	840 ± 60	8.2E43	3.9E44	4.1E23	QSO-2	BLAGN	3	2.810
76	60	53.04545	−27.73752	53.04550	−27.73755	0.2	9.8(±0.6)E-15	$0.20^{-0.03}_{+0.03}$	290 ± 30	1.2E44	1.6E44	1.8E22	QSO-1	BLAGN	3	1.615
86	57	53.05395	−27.87686	53.05400	−27.87691	0.2	4.7(±0.5)E-15	$0.75^{-0.06}_{+0.07}$	49 ± 9	5.4E43	2.5E44	3.8E23	QSO-2	HEX	3	2.562
88	56*a*	53.05516	−27.71136	53.05516	−27.71141	0.2	1.9(±0.1)E-14	$0.88^{-0.03}_{+0.03}$	700 ± 20	1.4E43	2.8E43	5.3E22	AGN-2	HEX	3	0.605
94	55	53.05837	−27.85022	53.05841	−27.85025	0.2	9.1(±0.7)E-15	$1.10^{-0.05}_{+0.06}$	140 ± 90	2.7E41	3.4E41	3.0E22	AGN-2	HEX	3	0.122
96	531	53.06012	−27.85305	53.06016	−27.85302	0.2	1.2(±0.3)E-15	$1.28^{-0.17}_{+0.29}$	100 ± 10	2.6E42	1.9E43	3.8E23	AGN-2	HEX	3	1.544
98	54	53.06070	−27.90600	53.06087	−27.90575	1.0	2.9(±0.4)E-15	$0.66^{-0.08}_{+0.09}$	< 80	4.0E43	1.5E44	2.9E23	QSO-2	HEX	3	2.361
103	53	53.06245	−27.85755	53.06245	−27.85755	0.0	3.4(±0.4)E-15	$0.29^{-0.05}_{+0.06}$	75 ± 25	5.2E42	6.5E42	1.0E22	AGN-1	BLAGN	3	0.675
109	206	53.06754	−27.65844	53.06750	−27.65850	0.2	1.8(±0.1)E-14	$0.15^{-0.03}_{+0.03}$	1350 ± 75	1.5E44	1.9E44	8.9E21	QSO-1	BLAGN	3	1.324
117	52	53.07141	−27.71758	53.07145	−27.71761	0.2	6.4(±0.5)E-15	$0.15^{-0.04}_{+0.04}$	1370 ± 90	7.3E42	8.1E42	3.2E21	AGN-1	BLAGN	3	0.569
122	87	53.07600	−27.87819	53.07604	−27.87816	0.2	6.3(±2)E-16	$0.24^{-0.13}_{+0.19}$	< 80	2.6E43	4.2E43	6.4E22	AGN-1	BLAGN	3	2.801
123	153	53.07641	−27.84866	53.07645	−27.84869	0.2	7.4(±0.7)E-15	$1.65^{-0.09}_{+0.12}$	130 ± 14	8.9E42	1.1E44	5.9E23	AGN-2	HEX	3	1.536
163	46	53.10487	−27.70522	53.10483	−27.70525	0.2	3.3(±0.4)E-15	$0.08^{-0.05}_{+0.06}$	500 ± 40	5.2E43	5.7E43	5.9E21	QSO-1	BLAGN	3	1.617
177	42*a*	53.11250	−27.68475	53.11250	−27.68475	0.0	6.9(±0.2)E-14	$0.14^{-0.01}_{+0.01}$	910 ± 70	1.4E44	1.6E44	4.3E21	QSO-1	BLAGN	3	0.734
179	41	53.11504	−27.69583	53.11508	−27.69583	0.1	1.2(±0.1)E-14	$1.38^{-0.06}_{+0.07}$	390 ± 10	6.9E42	2.2E43	1.2E23	AGN-2	HEX	3	0.668
188	202	53.12441	−27.85163	53.12441	−27.85161	0.1	3.2(±0.4)E-15	$1.02^{-0.08}_{+0.10}$	86 ± 11	3.2E43	4.1E44	1.0E24	QSO-2	HEX	3	3.700
191	39	53.12491	−27.75827	53.12525	−27.75852	1.4	1.3(±0.1)E-14	$0.22^{-0.02}_{+0.03}$	440 ± 60	8.3E43	1.0E44	1.3E22	QSO-1	BLAGN	3	1.218
193	78	53.12525	−27.75652	53.12525	−27.75655	0.1	2.2(±0.3)E-15	$0.08^{-0.06}_{+0.07}$	120 ± 10	9.4E42	1.0E43	2.6E21	AGN-1	BLAGN	3	0.960
195	38	53.12591	−27.75125	53.12625	−27.75150	1.4	7.2(±0.5)E-15	$0.09^{-0.03}_{+0.03}$	175 ± 30	1.6E43	1.7E43	2.5E21	AGN-1	BLAGN	3	0.738
197	563	53.13112	−27.77305	53.13141	−27.77350	1.9	<3.3E-16	< 0.71	370 ± 110	< 6.1E42	< 1.2E43	< 2.5E23	AGN-1	HEX	3	2.223
214	34*a*	53.14558	−27.91972	53.14566	−27.91977	0.3	3.6(±0.4)E-15	$0.38^{-0.06}_{+0.06}$	230 ± 10	8.4E42	1.2E43	1.9E22	AGN-1	HEX	3	0.839
219	901	53.14883	−27.82111	53.14883	−27.82111	0.0	7.0(±2)E-16	$1.11^{-0.19}_{+0.34}$	610 ± 10	3.8E42	3.8E43	8.3E23	AGN-1	HEX	3	2.578
229	32	53.15600	−27.66680	53.15612	−27.66675	0.5	2.4(±0.8)E-15	$0.12^{-0.12}_{+0.17}$	140 ± 30	4.2E42	4.5E42	3.1E21	AGN-1	BLAGN	3	0.664
230	31	53.15737	−27.87011	53.15741	−27.87011	0.1	8.9(±0.5)E-15	$0.17^{-0.03}_{+0.03}$	1150 ± 60	1.1E44	1.5E44	1.4E22	QSO-1	HEX	3	1.603
234	30*a*	53.15875	−27.66261	53.15887	−27.66250	0.6	1.6(±0.2)E-14	$-0.01^{-0.06}_{+0.08}$	560 ± 50	5.3E43	5.1E43	5.8E22	QSO-1	BLAGN	3	0.837
241	201*b*	53.16275	−27.74419	53.16225	−27.74427	1.6	2.1(±0.3)E-15	$0.66^{-0.08}_{+0.10}$	< 80	2.4E42	4.2E42	3.8E22	AGN-2	HEX	3	0.679
242	28	53.16283	−27.76713	53.16287	−27.76722	0.3	3.1(±0.4)E-15	$0.58^{-0.07}_{+0.08}$	250 ± 30	1.2E43	2.5E43	5.8E22	AGN-1	BLAGN	3	1.216
245	27	53.16533	−27.81408	53.16529	−27.81402	0.2	7.1(±0.6)E-15	$0.97^{-0.05}_{+0.06}$	150 ± 30	6.4E43	5.8E44	7.6E23	QSO-2	HEX	3	3.064
251	24	53.17445	−27.86736	53.17441	−27.86738	0.2	3.8(±0.5)E-15	$0.36^{-0.06}_{+0.06}$	110 ± 30	2.0E44	4.6E44	1.8E23	QSO-1	BLAGN	3	3.610
254	91	53.17850	−27.78400	53.17850	−27.78405	0.2	1.6(±0.3)E-15	$0.41^{-0.08}_{+0.09}$	< 80	5.8E43	1.5E44	1.9E23	QSO-1	BLAGN	1	3.193
261	21	53.18458	−27.88086	53.18466	−27.88091	0.3	6.8(±2)E-16	$0.10^{-0.12}_{+0.18}$	560 ± 100	6.1E43	7.6E43	3.3E22	QSO-1	BLAGN	3	3.471
275	19	53.19945	−27.69663	53.19966	−27.69666	0.7	1.3(±0.1)E-14	$0.19^{-0.04}_{+0.05}$	230 ± 35	2.7E43	3.1E43	6.2E21	AGN-1	BLAGN	3	0.733
278	268*a*	53.20512	−27.68050	53.20500	−27.68072	0.9	8.3(±2)E-15	> 1.36	2360 ± 600	1.2E43	7.1E43	> 2.7E23	AGN-2	HEX	3	1.222
286	15	53.22029	−27.85547	53.22033	−27.85555	0.3	5.4(±0.8)E-15	$0.27^{-0.04}_{+0.05}$	140 ± 50	3.3E43	4.6E43	1.9E22	AGN-1	BLAGN	1	1.227
290	101*a*	53.23116	−27.79763	53.23125	−27.79775	0.5	1.3(±0.3)E-15	$0.27^{-0.09}_{+0.12}$	80 ± 20	1.5E43	2.2E43	2.7E22	AGN-1	BLAGN	3	1.625
301	13	53.24595	−27.72766	53.24620	−27.72763	0.8	8.7(±0.8)E-15	$0.22^{-0.04}_{+0.05}$	270 ± 40	1.7E43	2.0E43	7.2E21	AGN-1	BLAGN	3	0.733
305	11	53.24929	−27.79669	53.24929	−27.79672	0.1	1.1(±0.6)E-14	$0.19^{-0.03}_{+0.03}$	100 ± 30	4.3E44	6.2E44	4.0E22	QSO-1	BLAGN	3	2.579
311	77	53.25641	−27.76175	53.25641	−27.76183	0.3	1.8(±0.4)E-15	$0.13^{-0.09}_{+0.11}$	380 ± 20	2.6E42	2.8E42	3.0E21	AGN-1	BLAGN	3	0.622
316	4*a*	53.26500	−27.75513	53.26512	−27.75525	0.6	6.4(±0.6)E-15	$0.29^{-0.04}_{+0.05}$	< 80	4.1E43	5.8E43	2.0E22	AGN-1	BLAGN	1	1.260

Table 3. Axis Ratios for the Optically–Dull Sample.

AID	Best Model	galfit b/a	sextr b/a	morphology notes
		AGN with redshifts $z < 0.5$ or $z > 0.8$		
65	34	0.24	0.34	dusty edge-on galaxy
84	-	int	0.60	small antennae
90	4	irr	—	irregular
131	1	pt	0.95	pt source
139	4	0.68	0.65	face-on spiral w bright bulge?
162	4	0.87	0.77	compact
164	2	0.74	0.76	face-on disk +br bulge
166	1	pt	0.35	faint pt. src
171	2	irr	0.51	irr with central bulge
216	34	0.63	0.49	compact w fuzz
221	4	0.68	0.77	compact w fuzz
259	-	irr	0.80	irregular
264	1	pt	0.86	compact w fuzz
271	4	0.62	0.59	bulge + fuzz
303	3	0.33	0.37	edge-on spiral
		AGN with redshifts $0.5 < z < 0.8$		
44	4	0.43	0.69	edge-on bulge+disk galaxy
48	-	irr	0.64	clumpy, v. faint
60	-	irr	0.38	compact src + fuzz
80	4	0.84	0.88	pt + fuzz
83	24	0.87	0.86	compact but extended
91	2	0.34	0.43	large clumpy spiral
126	13	pt	0.86	compact w some faint emiss
129	4	< 0.61	0.94	edge-on Sp w bright bulge
134	2	0.32	0.47	edge-on sp w bright bulge
146	2	0.26	0.41	edge-on sp w bright bulge
155	2	0.73	0.75	irr w bright bulge
157	4	0.50	0.57	somewhat inclined disk
161	4	0.85	0.90	compact
176	4	0.68	0.66	face-on Sp w central bulge
196	-	int	0.72	merger/interaction
212	24	0.89	0.84	compact
220	23	0.63	0.68	compact w fuzz
227	4	0.61	···	compact w fuzz
247	24	0.74	0.89	compact w faint fuzz
269	24	0.60	0.60	bright bulge +disk
276	23	0.78	0.75	compact+fuzz

Columns: (1) X-ray source identification from Alexander et al. (2003). (2) Best-fitting Galfit model (1=PSF, 2=Sersic, 3=PSF+Sersic, 4=bulge+disk). (3) Axis ratio from best-fitting Galfit model. (4) Axis ratio from best-fitting Source Extractor model. (5) Notes on galaxy morphology.

Table 4. Axis Ratios for the Optically–Active Sample.

AID	Best Model	galfit b/a	sextr b/a	morphology notes
		AGN with $z < 0.5$ or $z > 0.8$		
34	1	pt	0.99	slightly resolved
39	1	pt	0.93	point source
41	1	pt	0.98	point source + faint compact fuzz
43	1	pt	0.96	point source
68	1	pt	0.98	point source
76	1	pt	0.94	point source + faint compact fuzz
86	-	–	0.56	small interm spiral or irr
94	4	0.97	0.82	irr. intereaction?
96	4	irr	0.74	irregular
122	1	pt	0.91	point source
123	4	0.94	0.85	compact src + fuzz
163	1	pt	0.87	compact src
188	1	pt	0.83	point source
191	4	0.54	0.50	compact src + round fuzz
193	-	int	0.97	2 bright peaks + fuzz, merger?
197	-	irr	···	irr : bright core + offset fluff
214	-	**	0.69	face-on sp or interaction?
219	1	pt	0.49	faint point source + fuzz
230	1	pt	0.92	point source + faint compact fuzz
234	14	pt	0.89	point source + faint fuzz
242	1	pt	0.87	point source + fuzz
251	1	pt	0.99	point source
254	1	pt	0.91	point source
261	1	pt	0.96	point source
286	14	0.59[a]	0.70	psf + outer ring
		AGN with $0.5 < z < 0.8$		
66	3	0.86	0.92	point source + face-on disk
88	-	—	0.62	interacting face-on spiral?
103	4	0.86	0.93	round halo + possible inclined disk
117	-	0.88[a]	0.79	compact, round
177	3	0.90	0.93	psf + face-on disk
179	3	0.79	0.81	compact
195	-	0.85[a]	···	compact, round
229	4	0.88	0.90	bright center + fuzz
241	1	–	0.73	very faint fuzz

Columns: (1) X-ray source identification from Alexander et al. (2003). (2) Best-fitting Galfit model (1=PSF, 2=Sersic, 3=PSF+Sersic, 4=bulge+disk). (3) Axis ratio from best-fitting Galfit model. (4) Axis ratio from best-fitting Source Extractor model. (5) Notes on galaxy morphology.

[a]Galfit crashed, so the axis ratio was fit using IRAF's task **ellipse.**

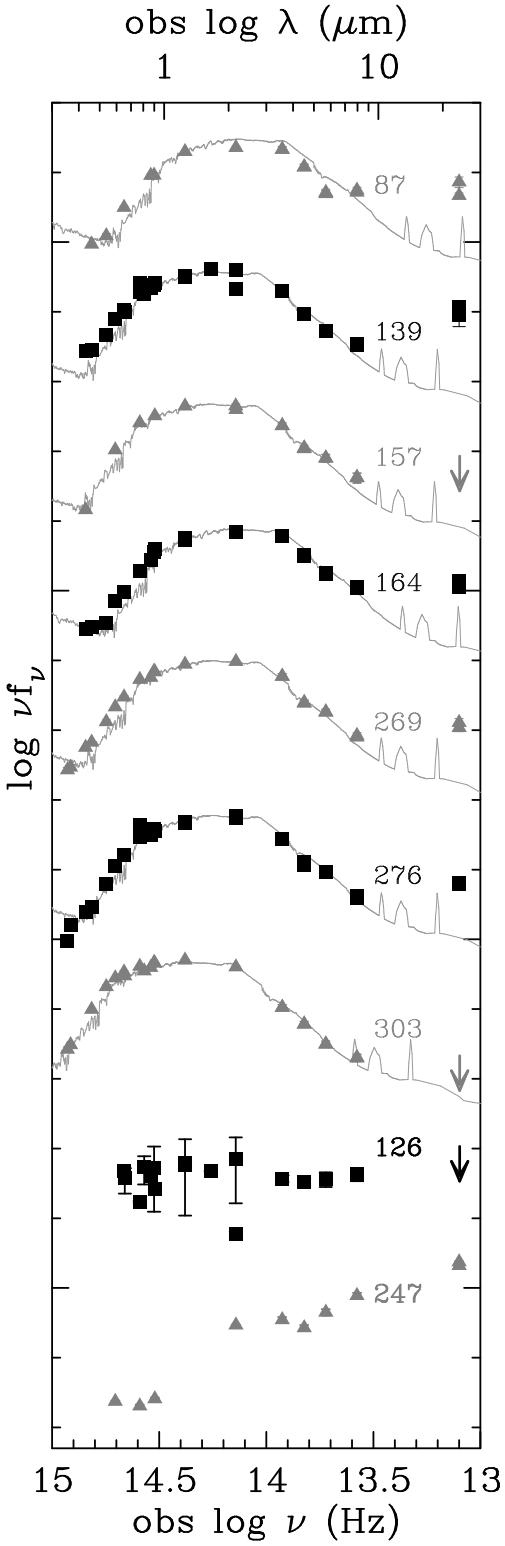

Fig. 1.— Spectral energy distributions of subsample A (optically–dull AGN with absorption-line (ABS) spectral classifications.) Wavelengths are as observed. For comparison, we plot templates of the SA galaxy VCC 1003 in the Virgo cluster (Devriendt et al. 1999).

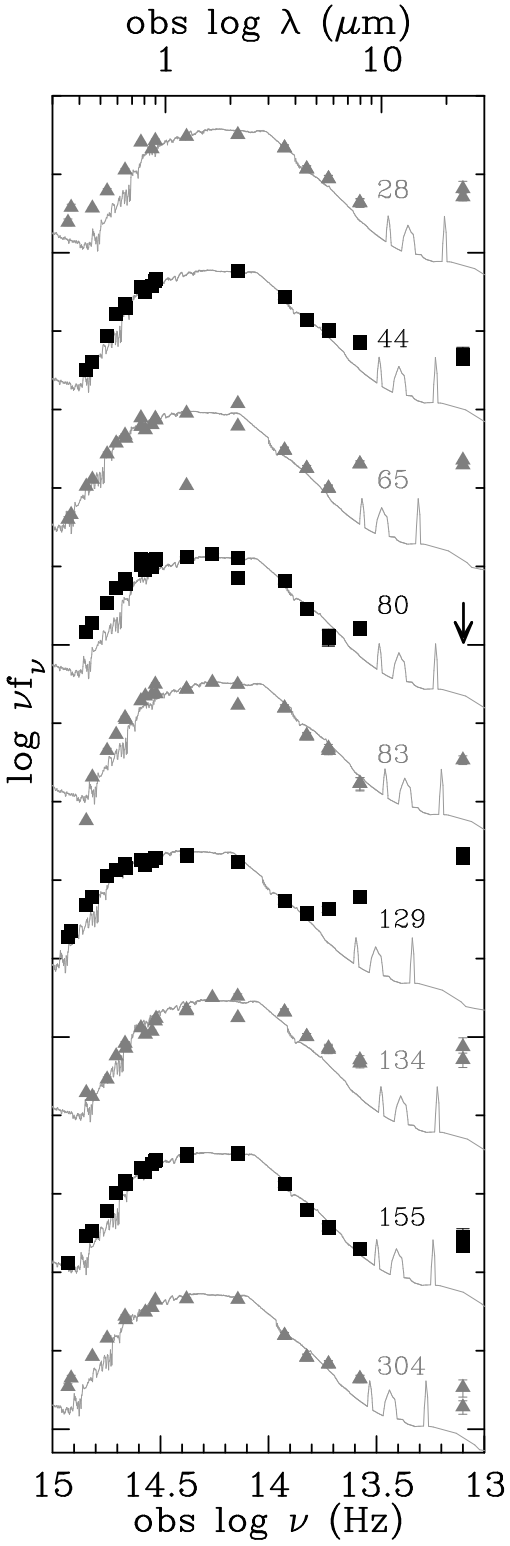

Fig. 2.— SEDs of subsample B. Wavelengths are as observed. For comparison, we plot the SA galaxy VCC 1003 in the Virgo cluster (Devriendt et al. 1999).

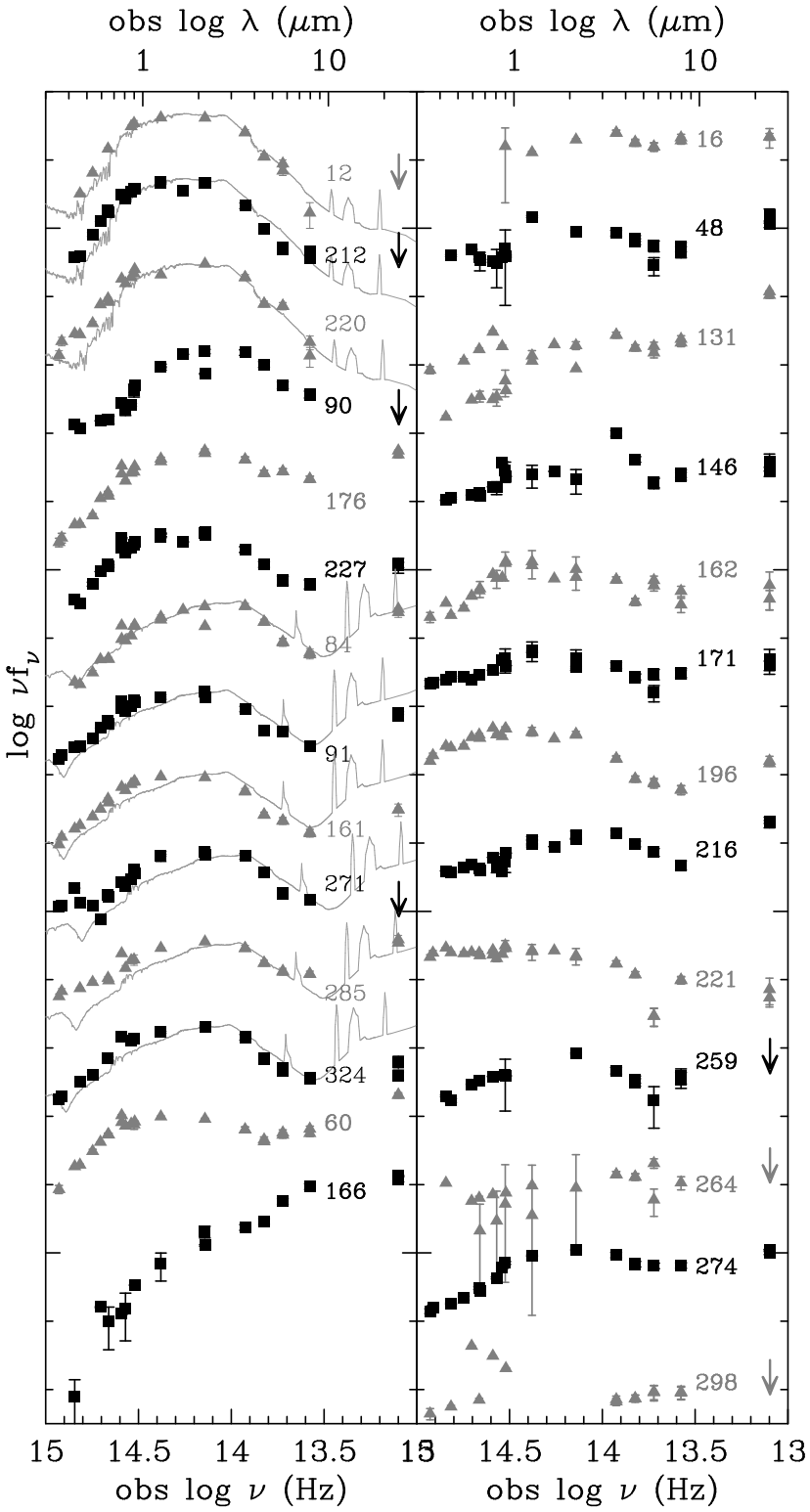

Fig. 3.— SEDs of the remaining optically-dull AGN. Wavelengths are as observed. Left panel, top to bottom: 3 old stellar pop SEDs; 3 intermediate SEDs; 6 young stellar pop SEDs; and 2 non-stellar rising-spectrum SEDs. Right panel: the non–stellar flat SEDs. For comparison, we plot the SA galaxy VCC 1003 with the old–type SEDs, and M82 with the young–type SEDs (Devriendt et al. 1999).

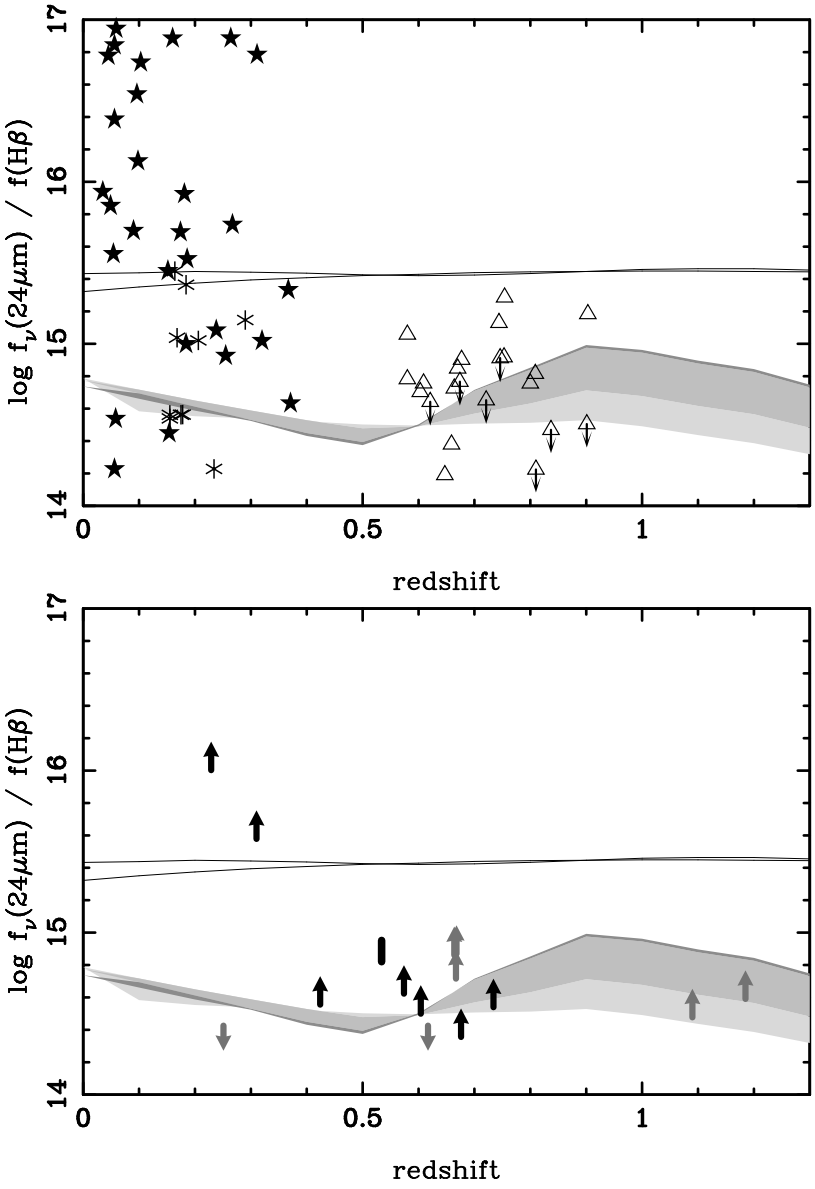

Fig. 4.— The observed $f_\nu(24\ \mu\mathrm{m})/f(H\beta)$ ratio. The upper panel shows the comparison samples: PG quasars (*asterisks*, 24 μm data from D. Hines, private communication, Hβ from the literature); radio quasars and FRII radio galaxies (*filled stars*, 24 μm data from Shi et al. 2005, Hβ from the literature); star-forming galaxies from the Extended Groth Strip (*triangles*, unpublished 24 μm data, Hβ from Lilly et al. 2003); and star–forming galaxy models with log L_{bol} =9–10 $L_\odot$(*darkest shaded region*); log L_{bol} = 10–11 $L_\odot$ (*lighter shaded region*); and log L_{bol} =11–12 $L_\odot$ models (*lightest shaded region*), all from Chary & Elbaz (2001). Solid lines show the expected K-corrections for median PG QSOs, from Elvis, Risaliti, & Zamorani (2002) and Haas et al. (2003), with arbitrary normalization. The bottom panel shows the optically–dull AGN from subsample A (*grey arrows*) and subsample B (*black arrows and bar*). The units of the y-axis are mJy/(erg s^{-1} cm^{-2}).

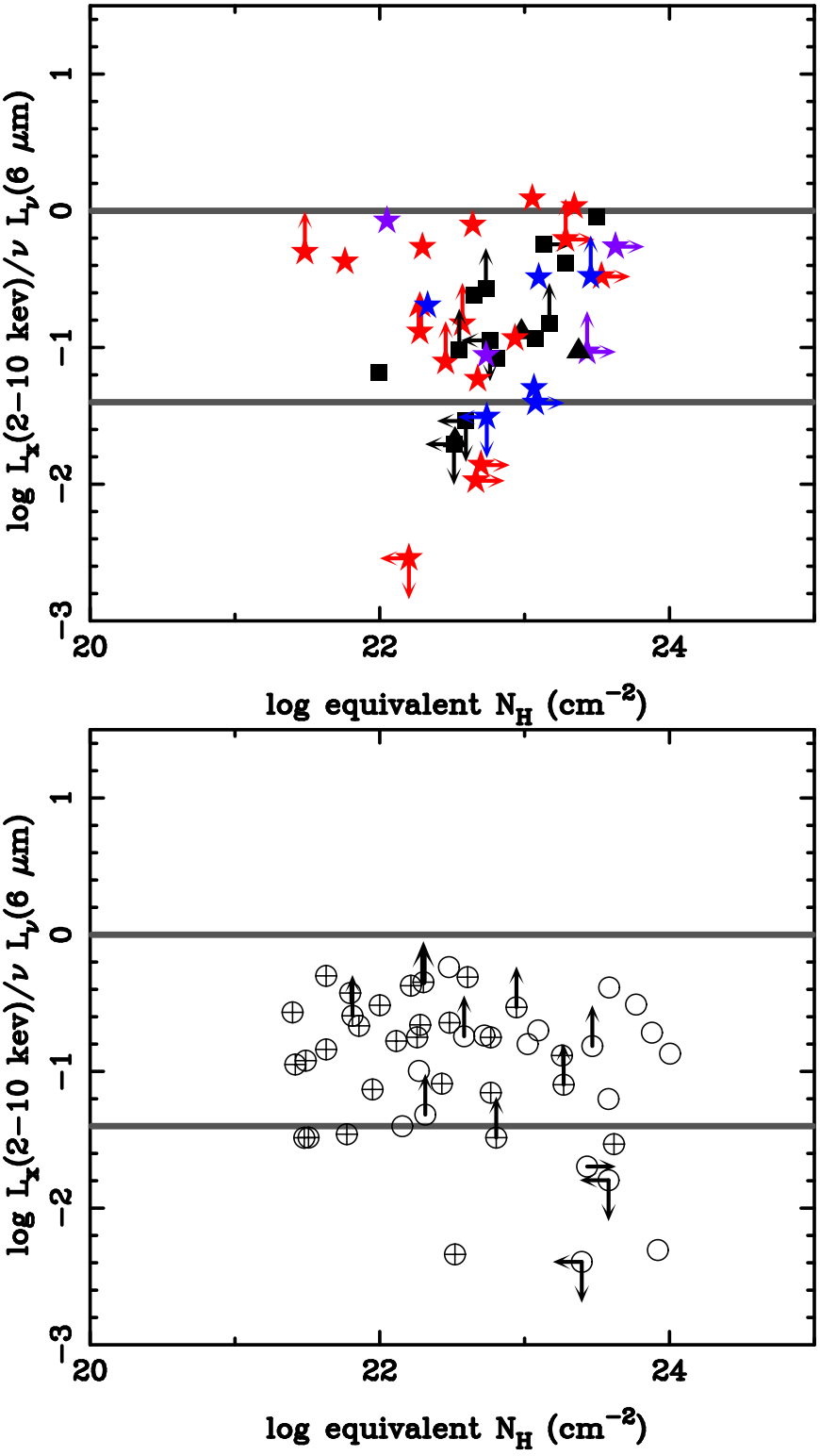

Fig. 5.— Ratio of 6 μm and X-ray luminosity versus inferred column density. Optically–dull AGN are plotted in the upper panel (symbols as in figure 8). Optically–active AGN, both BLAGN *(crossed circles)* and narrow-line AGN *(open circles)* are plotted in the lower panel. Horizontal lines mark the approximate luminosity ratio range observed in the low–redshift sample of Lutz et al. (2004) (see their figure 7.) Star–forming galaxies without AGN would have y-axis values in the range of -1.3 to -2.7, using data from Zezas et al. (2001) for three

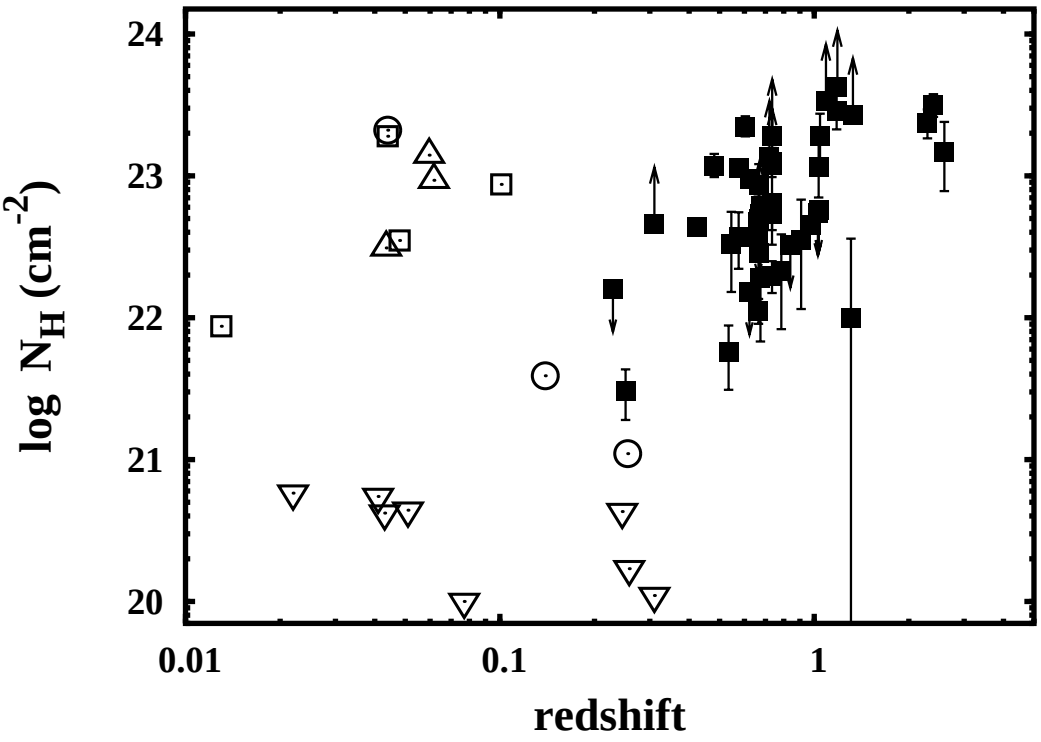

Fig. 6.— Column densities of optically–dull AGN. The low–redshift samples are: XMM serendipitous sources from (Severgnini et al. 2003) *(open circles)*; hard ASCA sources from Watanabe et al. (2002) *(up-pointing triangles)*; hard ASCA sources from Akiyama et al. (2003) with emission line equivalent widths < 10Å *(down-pointing triangles)*; and 5–10 keV BeppoSAX sources without AGN emission lines (La Franca et al. 2002) *(open squares)*, where we have used the (1.3–4.5 keV)/(4.5-10 keV) count ratios derived from Fiore et al. (2001) to estimate the column density. The higher redshift sources are our CDFS sample *(filled squares)*, with N_H values inferred from the flux ratio of the observed 2–8 keV and 0.5–2 keV bands (fluxes from Alexander et al. 2003).

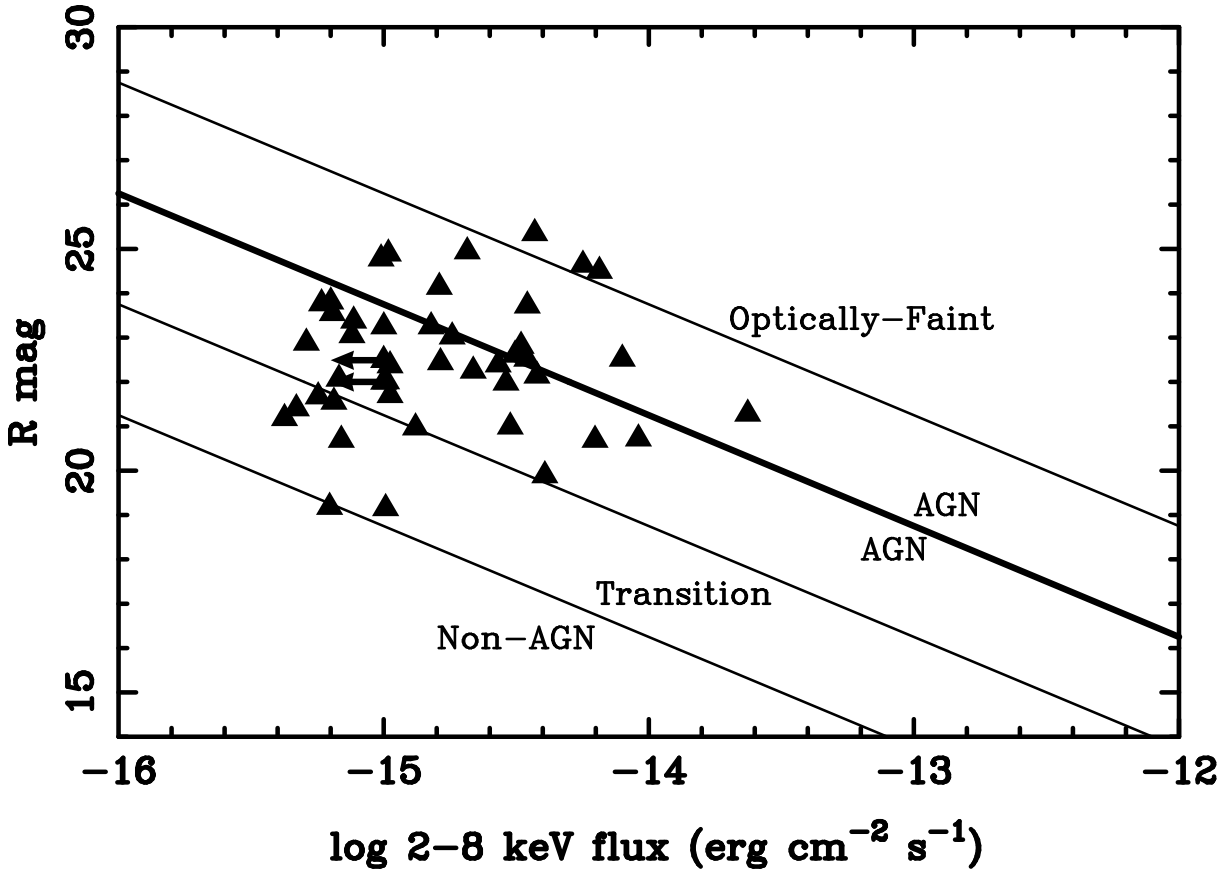

Fig. 7.— Observed R-band magnitude and X-ray flux for the optically–dull AGN. Data are from Giacconi et al. (2002). Lines mark flux ratios of F_x/F_R = 0.1, 1, and 10, following figure 3 of **?**.

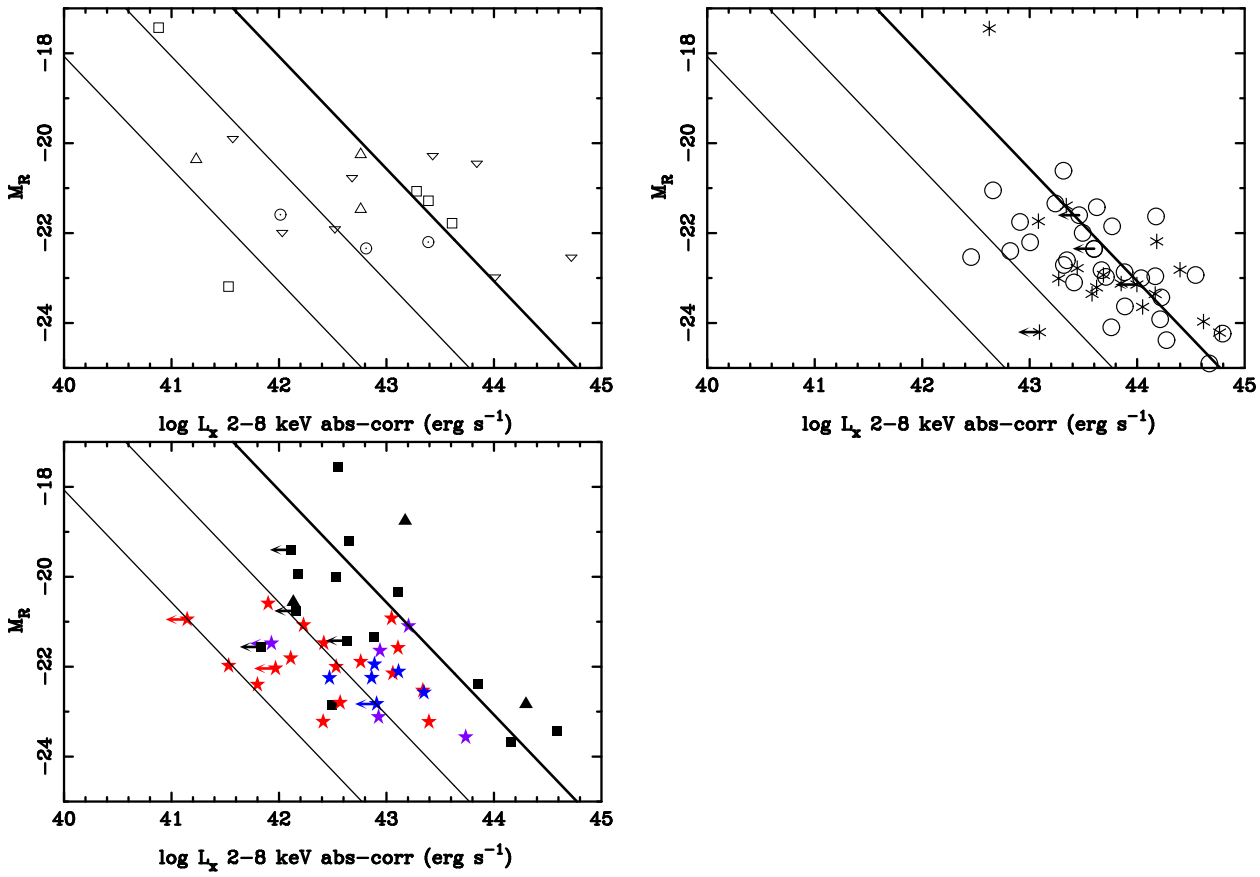

Fig. 8.— Absolute magnitude M_R versus absorption–corrected rest–frame 2–8 keV L_x. *panel 3a:* Low–redshift weak-line AGN samples, with symbols as in fig 6. *panel 3b:* Optically–active AGN from the CDFS, both broad-line *(asterisks)* and narrow-line *(circles)*. *panel 3c:* Optically–dull AGN from the CDFS, coded by SED type: old stellar pop*(red stars)*; intermediate *(purple stars)*; young stellar pop*(blue stars)*; flat in νf_ν*(black squares)*; rising in $\nu f_\nu$with increasing wavelength *(black triangles)*. The plotted X-ray luminosity is absorption–corrected, in the rest–frame 2–8 keV band, and is calculated from the observed 2–8 keV flux (Alexander et al. 2003) by assuming the intrinsic spectrum is a $\Gamma = 2$ power-law. M_R is calculated by linearly interpolating between bands that bracket the rest-frame R-band. The thick diagonal line shows the luminosity ratio of the composite Elvis, Risaliti, & Zamorani (2002) QSO SED. The thin diagonal lines mark ratios with 10 and 100 times higher optical luminosity.

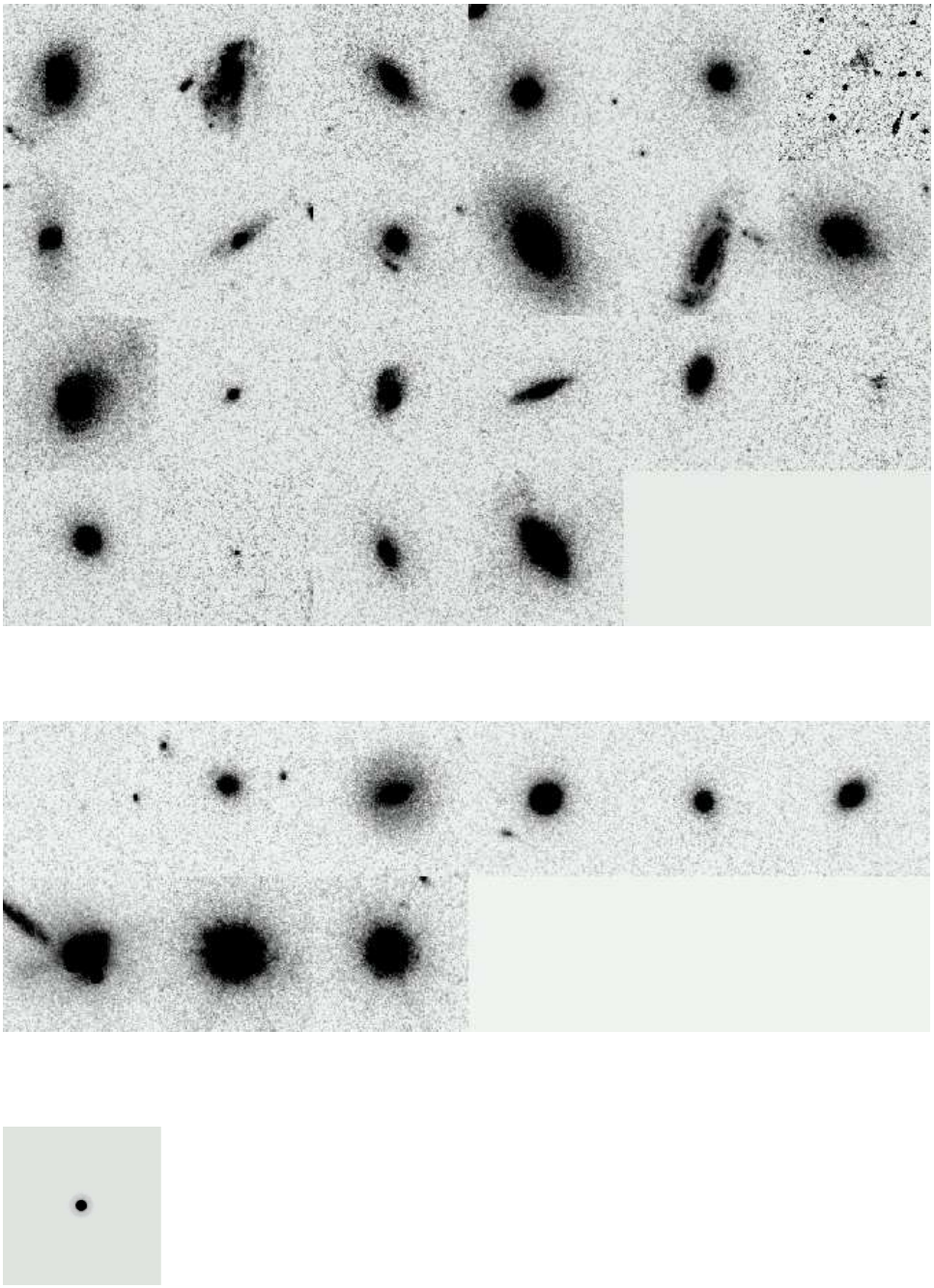

Fig. 9.— Postage stamps of the optically–dull AGN (top panel) and optically–active AGN (middle panel) at $0.5 < z < 0.8$. Data are ACS/HST i-band images from GOODS (Giavalisco et al. 2004); each postage stamp is 4.8″ on a side. Sources are plotted top to bottom, left to right in order of increasing absorption–corrected X-ray luminosity, as follows: Optically–dull AID: 139, 196, 157, 83, 212, 298, 60, 146, 80, 269, 91, 155, 276, 126, 176, 134, 22, 48 161, 247, 227, 44. Optically–active AID: 241, 229, 103, 117, 195, 179, 88, 66, 177. Also shown for comparison is the ACS/HST PSF in i-band, at the same pixel scale as the images (bottom panel).

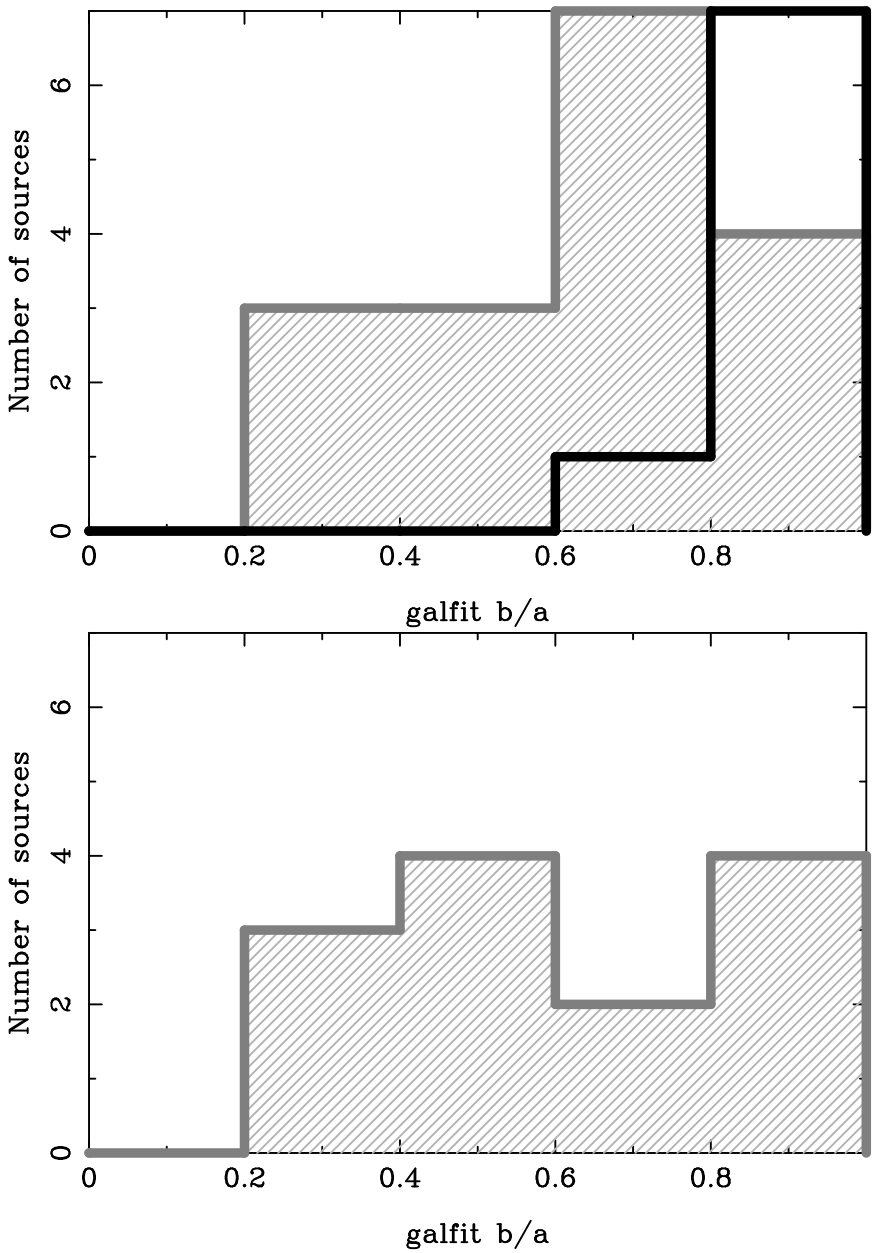

Fig. 10.— Axis ratio distributions of the optically–dull and optically–active AGN with redshifts $0.5 < z < 0.8$. Axis ratios are from Galfit models. Upper panel: The black histogram shows the distribution of the optically–active AGN; the hatched histogram shows the distribution of the optically–dull AGN. Lower panel: Axis ratios for the optically–dull AGN, if a nuclear point source is added to each.

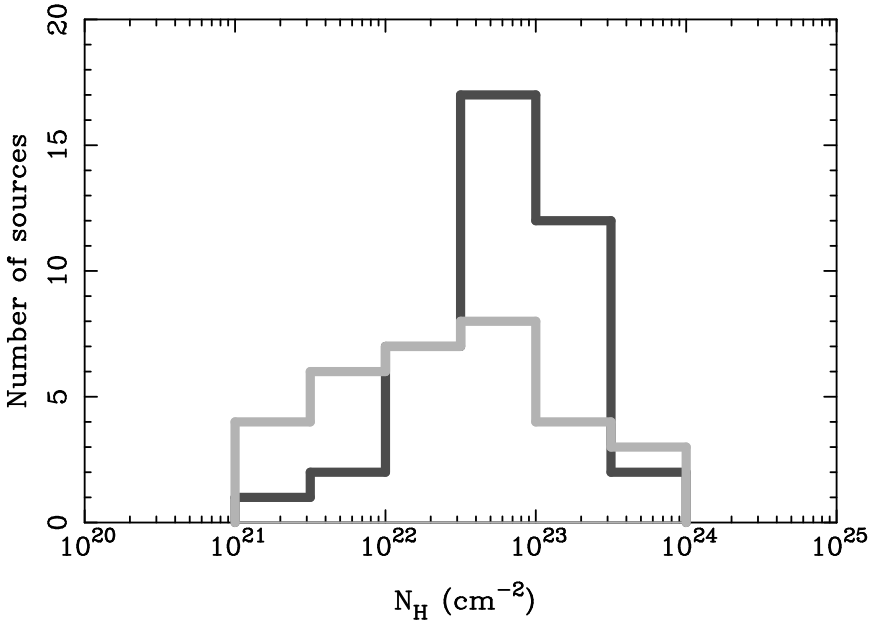

Fig. 11.— X-ray Column density distributions for the optically–dull *(dark histogram)* and optically–active *(light histogram)* AGN with absorption–corrected X-ray luminosities below 10^{44} erg s^{-1}. A K-S test shows the two distributions are different at the 95% confidence level; adding back in the QSOs increases the significance.